

Ground-based MAX-DOAS observations of NO₂ and H₂CO at Kinshasa and comparisons with TROPOMI observations

Rodriguez Yombo Phaka^{1,3}, Alexis Merlaud², Gaia Pinardi², Martina M. Friedrich², François Hendrick², Jean-François Müller², Jenny Trissevgeni Stavrakou², Isabelle De Smedt², Ermioni Dimitropoulou², Richard Bopili Mbotia Lepiba³, Edmond Phuku Phuati³, Buenimio Lomami Djibi³, Lars Jacob², Caroline Fayt², Michel Van Roozendael², Jean-Perre Mbungu Tsumbu³, and Emmanuel Mahieu¹

¹Institut d'Astrophysique et de Geophysique, UR SPHERES, Université de Liège, Liège, Belgique

²Royal Belgian Institute for Space Aeronomy (BIRA-IASB), Brussels, Belgium

³Université de Kinshasa, Faculté des Sciences/Dpt de Physique, Kinshasa, RDC

Correspondence: Rodriguez Yombo Phaka (rodriguez.yombophaka@student.uliege.be)

Abstract.

We present a database of MAX-DOAS (Multi-AXis Differential Optical Absorption Spectroscopy) ground-based observations of NO₂ and H₂CO tropospheric vertical column densities (VCD_{tropo})^{Add} performed for the first time in the city of Kinshasa. These measurements were conducted between November 2019 and July 2021 and processed using the standardized inversion tools developed in the ESA FRM4DOAS (Fiducial Reference Measurements for Ground-Based DOAS Air-Quality Observations) project. The retrieved geophysical quantities are used to validate column observations from the TROPospheric Monitoring Instrument (TROPOMI) in Kinshasa. In the validation, we experiment three different comparison cases of increasing complexity. In the first case, a direct comparison between MAX-DOAS observations (hourly average of MAX-DOAS VCD_{tropo} at overpass)^{Add} (average +/- 60 minutes around overpass)^{Del} and TROPOMI shows an underestimation of TROPOMI with a median bias of -39% (slope $s=0.26^{Del}0.67^{Add}$ and correlation coefficient $R=0.41^{Del}0.71^{Add}$) for NO₂ monthly comparison^{Add} and $-26\%^{Del}-39\%^{Add}$ ($s=0.24^{Del}0.68^{Add}$ and $R=0.28^{Del}0.79^{Add}$) for H₂CO monthly comparison^{Add}. The second case takes into account the different vertical sensitivities of the two instruments and the a priori profile. ~~We note a slight decrease of the biases and a strong improvement of the linear regression parameter, about -35% ($s=0.72$ and $R=0.74$) for NO₂ and 1% ($s=1.01$ and $R=0.66$) for H₂CO.~~^{Del} We note significant changes of the mean bias for both NO₂ -12% ($s=0.64$ and $R=0.68$) and H₂CO +11% ($s=1.00$ and $R=0.73$)^{Add}. The third case builds on the second case by considering also the direction of sight of the MAX-DOAS. For this third case, we find a median bias of +44% ($s=0.77$ and $R=0.48$) for NO₂ and a median bias of +4% ($s=0.90$ and $R=0.55$) for H₂CO. However this case is impacted by low sampling and is considered as less reliable. The findings from this study underscore the significance of employing a realistic a priori profile in TROPOMI column extraction, particularly within heavily polluted urban zones like Kinshasa. The investigation also highlights the necessity for prudence when integrating the MAX-DOAS line of sight due to the noise generated during subsampling and the limited horizontal sensitivity of MAX-DOAS observations. Importantly, the study further reveals the pronounced pollution levels of NO₂, H₂CO, and aerosols in both the city of Kinshasa and its adjacent regions, underscoring the imperative for consistent monitoring and effective regulatory measures by regional authorities.^{Add}

The third case, which is considered more realistic than the first two, builds on the second case by considering also the direction of sight of the MAX-DOAS. For this third case, we find a bias of -2% ($s=1.09$; $R=0.59$) for NO_2 and 13% ($s=1.51$; $R=0.60$) for H_2CO . Those results indicate a large impact of the vertical sensitivity and horizontal heterogeneity in this validation process at this site. In order to evaluate the capability of the GEOS-Chem model in this region, we performed the comparisons between TROPOMI and the simulations made for 2020. We found a bias of 16% ($s=0.42$ and $R=0.80$) for NO_2 and bias of 61% ($s=0.05$ and $R=0.24$) for H_2CO .^{Del}

30 1 Introduction

The population explosion in Africa is a growing source of environmental problems. In particular, many African cities are increasingly affected by air pollution, so that air quality in African urban areas is expected to deteriorate in the coming decades with a strong impact on human health (Lioussé et al., 2014). NO_x (sum of NO and NO_2) and formaldehyde (H_2CO) are important markers of this pollution. These compounds are also strongly emitted by fires and the biosphere; H_2CO is also considered an excellent marker of biogenic volatile organic compounds (VOCs) emissions (Stavrakou et al., 2009; Bauwens et al., 2016).^{Add} In the presence of VOCs ~~volatile organic compounds (VOCs) among them~~ H_2CO ^{Del}, high NO_2 concentrations lead to increased formation of O_3 and aerosols (Crutzen, 1979). H_2CO plays a primary role on the oxidative capacity of the atmosphere and affects the global CO balance (e.g., Fortems-Cheiney et al., 2012; Cheng et al., 2018). The VOCs and NO_2 react in a non-linear manner to form O_3 in the atmosphere (eg., Seinfeld and Pandis (1998)).^{Add}

40 At the global scale, the main sources of NO_x are combustion processes associated with traffic, industrial activities, and home heating whereas H_2CO is formed during the atmospheric oxidation of methane and non-methane volatile organic compounds (NMVOCs) of biogenic, pyrogenic, and anthropogenic sources origin (Seinfeld and Pandis, 1998). In tropical regions, particularly in Central Africa, major sources impacting NO_x and H_2CO include the seasonal biomass burning, the use of charcoal in cooking, and road traffic, generally dominated by old smoke emitting vehicles (Marais and Wiedinmyer, 2016).
45 At present, relatively few studies have addressed NO_2 and H_2CO sources in Central Africa, and in-situ measurements are generally lacking in tropical regions. Although nadir-looking UV-visible spaceborne sensors (e.g. TROPOMI) do sample this region, current satellite datasets present biases with respect to independent measurements. For example, TROPOMI H_2CO columns tend to systematically underestimate ground-based infrared remote-sensing data in polluted regions (Vigouroux et al., 2020). Regarding tropospheric NO_2 , columns validation studies indicate moderate underestimations at polluted mid-latitudes sites (e.g. Dimitropoulou et al. (2020); Zhao et al. (2020); Tack et al. (2021); Verhoelst et al. (2021); Poraicu et al. (2023)).
50 However, satellite measurements are poorly characterized in tropical regions.

The Democratic Republic of Congo (DRC), a country in the heart of the Congo Basin, has multiple sources of air pollutants. Alone, it accounts for 54% of the Congo Basin rainforest affected by deforestation due to expansion of agriculture and increasing demand for firewood (Mayaux et al., 2013). The associated emissions can be observed from space by satellite. For example, De Smedt et al. (2015) found that H_2CO column hotspots associated with vegetation fires in the region are among the highest in the world. Measurements in Bujumbura (Burundi) using the MAX-DOAS (Multi-AXis Differential Optical Absorp-

tion Spectroscopy) technique, have shown that the local atmospheric composition is influenced by biogenic VOC emissions from the DRC (Gielen et al., 2014), even though this site is relatively far away from emission sources.

Kinshasa, the capital of the DRC, a large and rapidly expanding ~~megalopolis~~^{Del} ~~megacity~~^{Add} of 12 million inhabitants in 2016 expected ~~at~~^{Del} ~~to reach~~^{Add} 20 million by 2030 (UN, 2016), is not spared by air pollution problems (McFarlane et al., 2021). It experiences a rapid increase in the number of motorcycles, a fleet dominated by old vehicles, poorly managed roads largely unpaved and, much like other large cities in Central Africa, poor quality fuel. It is also surrounded by the vast forested areas of the Congo Basin and most of its population uses charcoal for cooking. A recent study by Vohra et al. (2022), based on space-based observations has shown that several large African megacities, including Kinshasa, are experiencing significant annual increases in NO₂ due to emerging anthropogenic sources. It can also be seen that Kinshasa city center, where most activities take place (traffic, markets, businesses, etc), is more affected than other parts of the city. In spite of the reported pollution increases, the lack of routine monitoring impedes the development of efficient policies aiming to improve the quality of the air.

In May 2017, a single-axis DOAS (Differential Optical Absorption Spectroscopy) system was installed on the roof of the Faculty of Sciences of the University of Kinshasa (UniKin) as part of a collaboration with the Belgian Institute for Space Aeronomy (BIRA-IASB). ~~Based on measurements obtained from this instrument operated~~^{Add} ~~Based on this instrument, which was operated~~^{Del} from 5 May 2017 to 1 November 2019, Yombo Phaka et al. (2021) identified the presence of a clear annual cycle in NO₂ concentrations with higher values during the dry season. A good correlation was found with satellite measurements, although the latter seemed to be biased low compared to the ground based-measurements. In November 2019, the single-axis instrument was replaced by a new MAX-DOAS (Multi-AXis DOAS) system built at BIRA-IASB, significantly increasing the information content of the measurements. The geophysical quantities extracted from these measurements are tropospheric column densities (VCD_{tropo}) and vertical profiles of NO₂ and H₂CO, as well as aerosol optical depths (AODs) and extinction profiles.

We present measurements conducted from November 2019 to July 2021. Vertical columns of NO₂ and H₂CO are used to validate co-located measurements from the TROPOMI instrument on board the Sentinel-5P (S5P) satellite and the AOD measured by the MAX-DOAS instrument is compared with MODIS satellite data. ~~We also present comparisons between TROPOMI and GEOS-Chem model simulations, in view of assessing the model capability in this region.~~^{Del} This manuscript is subdivided into 4 sections: Section 2 presents the observation site, the retrieval methodology and input parameters; Section 3 presents the resulting dataset as well as comparisons of TROPOMI with ~~the GEOS-Chem model simulations~~^{Del} ~~MAX-DOAS~~^{Add}; Section 4 discusses the differences between the datasets, and the final section presents the conclusions.

85 2 Observations and data sets

2.1 Site description and instrumental setup

Figure 1 presents the ~~MAX-DOAS~~^{Add} instrument installed on the roof of the Faculty of Science of the University of Kinshasa (UniKin: -4.42° S, 15.31° E, 315 m a.s.l.) and its surroundings. On clear sky days during the dry season, the Lumumba tower is visible at 5.7 km from the site. During the wet season, Brazzaville is visible at about 16 km from the site. The reduction in

90 visibility observed in the dry season is due to the presence of aerosols. The UniKin site is located about 5 km from downtown Kinshasa and about 10 km from the Congo River. More details on the city of Kinshasa and its characteristics are described in Yombo Phaka et al. (2021). ~~The instrument consists of an optical head (represented in Fig. 1, panel c) equipped with a scanning mirror, controlling the elevation angles (0, 1, 2, 3, 4, 5, 6, 7°, 8°, 15°, 30°, 45°, 88°). The scattered sunlight collected by the telescope is redirected by means of an optical fiber to an Avantes spectrometer (ULS-2048-XL) located in the main building.~~
95 ~~The spectrometer covers the UV-Visible wavelength range (290-550 nm) and its spectral resolution is 0.7 nm full width at half maximum (FWHM). An on-board computer (PC104) ensures the operation of the whole system (automatic recording of spectra and control of the telescope).~~^{Del}

The MAX-DOAS is an upgrade of the single-axis DOAS instrument described in more detail in our previous study (Yombo Phaka et al., 2021). The spectrometer is an Avantes ULS2048-XL with a spectral range of 280-550 nm and a spectral resolution
100 of 0.7 nm (Full Width at Half Maximum), Light enters the spectrometer through a lens connected to an optical fiber 600 μ in diameter. The upgrade first consisted in installing this spectrometer and a single-board computer (PC-104) in a box, which is air-cooled with a fan and equipped with a temperature sensor. This box is located under the roof of UniKin. Secondly and more importantly, we added an optical head on the roof, to perform elevation scans. This optical head is based on a home-made box of dimensions $22 \times 14 \times 8 \text{ cm}^3$ mounted on a pod at 45° and pointing 5° West of the North, i.e. towards the city. Light
105 enters the box through a fused silica window and hits a flat elliptical mirror of minor axis 26.97 mm coated with enhanced aluminum. This mirror is attached to a HITEC servomotor (HS-7985MG) and scans between the horizon and zenith at multiple angles above the horizon ($0^\circ, 1^\circ, 2^\circ, 3^\circ, 4^\circ, 5^\circ, 6^\circ, 7^\circ, 8^\circ, 15^\circ, 30^\circ, 45^\circ, 88^\circ$). The mirror reflects the light to a fused silica plano-convex lens of 25 mm diameter and 50 mm focal length, which focuses the light on the optical fiber. In each mirror position, we accumulate light for 50 seconds leading to a total scan time in about 10 minutes.^{Add}

110 2.2 Retrieval methodology

The retrieval of NO_2 and H_2CO tropospheric vertical columns densities is performed using tools developed as part of the FRM4DOAS project (Fiducial Reference Measurements for Ground-Based DOAS Air-Quality Observations
(<https://frm4doas.aeronomie.be/>). FRM4DOAS is an international project funded by the European Space Agency (ESA) and aims at harmonizing and standardizing the data retrieval from MAX-DOAS instruments operated within the International Net-
115 work for the Detection of Atmospheric Composition Change (NDACC). It incorporates community-based retrieval algorithms into a fully traceable, automated and quality controlled processing environment.

Spectra recorded by the instruments are delivered in NetCDF4 format to a BIRA-IASB hosted ftp server. The automated analysis steps which are performed depend on the type of measurement (zenith only or MAX-DOAS) and on the spectral coverage of the instrument and are predefined for each instrument. However, the processing always starts with the production
120 of differential slant column densities (dSCDs) applying the QDOAS analysis tool (Danckaert and Fayt, 2017). The settings for QDOAS depend on the further processing, tropospheric or stratospheric retrieval (stratospheric NO_2 or total ozone column), as well as on instrument specifications and are described in the FRM4DOAS ATBD (FRM4DOAS ATBD, 2017).

For the specific case of the MAX-DOAS retrievals in Kinshasa, we use four fitting windows: one for the retrieval of NO₂ dSCDs (in the visible spectral range), one for the retrieval of H₂CO dSCDs (in the UV) and two for the retrieval of dSCDs of the oxygen-collision complex O₂-O₂ denoted by O₄ (in both visible and UV ranges). Details of the retrieval settings are summarized in Table 1.

Figure 2 illustrates typical QDOAS fits in the four windows, for a spectrum recorded on ~~15-May-2020 at 13:18 UTC~~^{Del} 20 February 2020 at 09:10 UTC^{Add}. In each panel, the blue line shows the measured differential optical densities as a function of wavelength and the black curve shows the molecular cross-sections scaled to the measured data.

From the DOAS fits, the FRM4DOAS system implements two MAX-DOAS retrieval algorithms: MAPA (Beirle et al., 2019), which is based on a parametrization of the retrieval profile shape and a Monte-Carlo approach for the inversion and MMF (Friedrich et al., 2019), an optimal estimation-based algorithm using the radiative transfer code VLIDORT (Spurr, 2013) as forward model. Both inversion algorithms have been extensively tested and validated using synthetic (Frieß et al., 2019) and real data (Tirpitz et al. (2021), Karagkiozidis et al. (2022)).

In the framework of FRM4DOAS, the current strategy is to use both codes to produce independent profile and column data sets. For operational delivery, only MMF data selected for their consistency with corresponding MAPA results are retained. These results are submitted to the NDACC/RD repository¹ and to the ESA EVDC data base (<https://evdc.esa.int/search/>). Both MMF and MAPA codes implement a two-step retrieval approach for trace gas profile retrieval. In the first step, the aerosol profile is determined based on a set of O₄ dSCDs. In the second step, the retrieved aerosol profile is used to constrain the radiative transfer simulations needed for the trace gas retrieval. This implies that O₄ dSCDs must be determined in the visible wavelength region for NO₂ and in the UV for H₂CO retrieval. Note that, in this work, we only considered MMF due to inconsistencies in the MAPA aerosol retrievals for our Kinshasa spectra.

Currently, in FRM4DOAS, MAPA is mainly used as a quality check, but it does not provide averaging kernels. Due to a sampling effect, using MAPA as a quality check for H₂CO introduces a bias in the statistics. Higher VCDs are more likely to be flagged out, leading to discrepancies between MAPA and MMF. When assessing Aerosol Optical Depths (AODs), it becomes evident that MMF-produced AODs closely align with MODIS AODs, while MAPA-derived AODs consistently surpass both MMF and MODIS. We therefore opted to exclude MAPA from this study. Consistency is maintained by applying the same flagging criteria to NO₂. Only MMF values for which the quality assurance (QA) is lower than 2 were used. Three conditions should be met to establish this flagging (QA < 2). Firstly, scans with a degree of freedom (dof) below 1.3 are excluded. Secondly, all scans with an average root-mean-square (RMS) (between measured and simulated dSCDs) larger than 4 times the QDOAS estimated dSCD error are excluded. Furthermore, due to lack of good a priori knowledge for the aerosols, two aerosol retrievals are performed (differing by a factor 10 in AOD). If the retrieved aerosol profile agrees well, only one trace gas retrieval is performed and no extra test is applied. If however the retrieved aerosol profile differs more than 10% (as average partial AOD in each layer), the trace gas profile is performed with both aerosol profiles and all scans for which the retrieved VCD differs more than 10% are flagged as invalid.^{Add} Tables 2 summarizes the main settings used for the NO₂ and H₂CO retrievals based on MMF. Note that regarding aerosol parameters (single scattering albedo and phase function

¹<https://www-air.larc.nasa.gov/missions/ndacc/data.html?RapidDelivery=rd-list>

moments) and surface albedo the same default settings were used in both ~~algorithms~~^{Del} ~~molecules~~^{Add}. For the meteorological input parameters, the FRM4DOAS retrieval chain uses an interpolation of a monthly climatology at each station, extracted from global meteorological reanalysis of the European Centre for Medium-Range Weather Forecasts (ECMWF) from 1995 to 160 2016 produced by Max Planck Institute for Chemistry (MPIC). An example of retrieval scan including the measurement for ~~15 May 2020 at 13h18 UTC~~^{Del} 1 March 2020 at 13:13 UTC^{Add} is displayed in Fig. 3. Vertical concentration profiles (Fig. 3 b, d, f and h) retrieved by MMF and corresponding averaging kernels (AKs) (Fig. 3 a, c, e and g) are displayed. Inserts the AK panels, we show the degree of freedom for signal (dof) and the error bars included in the profile concentration plots show the total errors, including random error components such as smoothing and noise error from the inversion, as well as systematic 165 uncertainties due to absorption cross section; namely 3% for NO₂ (Vandaele et al., 1998), 9% for H₂CO (Pinardi et al., 2013) and 20% for aerosol properties (Wagner et al., 2009). A priori profiles are represented next to retrieved profiles. The AKs indicate that the inversions are sensitive from the surface up to about 2.5 km.

2.3 TROPOMI data

TROPOMI is a nadir imaging spectrometer that measures reflected sunlight in the ultraviolet, visible, near-infrared, and short-wave infrared spectral ranges (Veeffkind et al., 2012). The TROPOMI overpasses over Kinshasa occur around 12:30 UTC (13:30 170 LT). Its spatial resolution at nadir is 5.5 km × 3.5 km. TROPOMI data used in this work are based on the ~~S5P-PAL~~, which stands for Sentinel-5P Products Algorithm Laboratory^{Add} ~~S5P-PAL~~^{Del} product for NO₂ (<https://data-portal.s5p-pal.com/>) and the reprocessed (RPRO v1.1) and off-line (OFFL: v2.1.3) for H₂CO. ~~The NO₂ product from S5P-PAL is reprocessed with the same processor as version 2.3.1, covering the period from 01 May 2018 to 14 November 2021.~~^{Add} For more technical 175 details on the two products used, the reader is referred to the Algorithm Theoretical Basis Document (ATBD), available at <http://www.tropomi.eu/data-products/> (last access: 25 May 2023) ^{Add}. We selected only those pixels associated with a quality value (qa-value > 0.75 for NO₂ and qa-value > 0.5 for H₂CO) following the recommendations of van Geffen et al. (2022) and of De Smedt et al. (2021). ~~Only pixels within a radius of 20 km around the observation site were selected for comparisons between TROPOMI and ground-based (GB) measurements.~~^{Del} ~~For comparisons with the GEOS-Chem model as described in~~ 180 ~~Sect 3.3, satellite data are averaged over the model cell around the study area (3.05–5.02°S, 13.8–16.3°E)~~^{Del}.

This TROPOMI data set has been exploited in this work in three ways. Firstly, we apply the oversampling technique to this data set in order to provide information on the horizontal distribution of the two target compounds around the measuring site (see next paragraph). Secondly, direct comparisons between the standard TROPOMI product and ground-based measurements are performed. Thirdly, comparisons are performed that take into account differences in the vertical sensitivity of the MAX-DOAS and TROPOMI instruments (see Sect 2.5). Note that for these comparisons with ground measurements, only pixels 185 within a radius of 20km around the observation site were selected. The choice of 20 km was made for three main reasons: (1) consistency with the horizontal sensitivity of the MAX-DOAS instrument, which generally varies between 3 and 20 km depending on visibility conditions, as shown in Fig. 1, (2) reduction of random uncertainty in TROPOMI data, especially for H₂CO, as tested by Vigouroux et al. (2020), (3) consistency with Yombo Phaka et al. (2021), a study similar to this one and 190 also other studies such as Pinardi et al. (2020); Irie et al. (2008), having tested these selection criteria for the case of NO₂.^{Add}

The oversampling technique consists in long-term averaging of the satellite data on a very fine spatial grid, $0.01^\circ \times 0.01^\circ$ (1×1 km²), in a small domain around the station (4° - 5° S, 14.8° - 15.8° E). In this way, a high signal-to-noise ratio is achieved at high spatial resolution, at the expense of temporal resolution. We use TROPOMI data between January 2020 and June 2021, i.e. roughly the period of the MAX-DOAS measurements at Kinshasa. The technique takes advantage of the variable offset and geometry of the satellite measurement from day to day. This technique has been previously applied to SO₂ and NO₂ (de Foy et al., 2009; McLinden et al., 2012) and H₂CO (e.g., Zhu et al. (2014) from OMI. We oversample both H₂CO and NO₂ vertical columns from TROPOMI. The column measurement for a given TROPOMI pixel is assumed to apply to a circle defined by the center of the pixel and a radius of 3.5 km. In this way, each $0.01^\circ \times 0.01^\circ$ pixel accumulates ≈ 200 measurements over the considered time period.^{Add}

The resulting distributions on Fig. 4 show clear hot spots over the city of Kinshasa, with maximum values of $\approx 4.75 \times 10^{15}$ molecules cm⁻² and $\approx 16.0 \times 10^{15}$ molecules cm⁻² for NO₂ and H₂CO, respectively. Although the instrument is located outside the most polluted area, the instrument points towards downtown Kinshasa, where NO₂ and H₂CO levels are highest. These values are even higher when viewed in the direction of the MAX-DOAS, i.e. to the north of the city, precisely in downtown Kinshasa.^{Add}

2.4 GEOS-Chem model data

We use a standard full chemistry simulation performed with the Goddard Earth Observing System chemistry (GEOS-Chem) model. GEOS-Chem is a 3D chemistry model that calculates local variations in atmospheric concentrations due to emissions, chemistry and deposition. The GEOS-Chem model has seen multiple applications across various regions of Africa (Lunt et al. (2019), Marais et al. (2019), and Bockarie et al. (2020)).^{Add} We use version 12.0.2 (<https://doi.org/10.5281/zenodo.1455215>) runs implementing MERRA-2 assimilated meteorological fields at a horizontal resolution of $2^\circ \times 2.5^\circ$ (latitude/longitude) on a vertical grid of 72 levels, up to 0.01 hPa (about 80 km). Emission inventories are taken into account using the Harvard Emission Component (HEMCO; Keller et al. (2014)) version 2.1.008 available in this version of the model. Our simulation includes EDGAR v4.3 for fossil fuel emissions, EMEP and NEI2011 for regional anthropogenic emissions, GFED v4 for fire emissions, MEGAN v2.1 for biogenic emissions, and RETRO for Non-Methane Volatile Organic Compounds (COVNM) emissions. In particular, the Diffuse and Inefficient Combustion Emissions in Africa (DICE-Africa) inventory is implemented to provide African anthropogenic emissions as in Marais and Wiedinmyer (2016). DICE-Africa includes emissions from domestic and commercial use of wood from forests, household combustion of harvest residues, charcoal production and use, gas flaring, adhoc oil refining (Niger Delta only), kerosene use, diesel/petrol generators, and vehicles (including motorcycles). We use in the present study global multi-year simulations initiated in 2010, meaning that the years investigated here are unaffected by the initial conditions. The model outputs are saved every 2 hours.

2.5 Intercomparison methodology^{Add}

Three different cases are explored in this study to compare the TROPOMI observations to those of MAX-DOAS.

Case 1: We select all TROPOMI pixels within a radius of 20 km around the observation site and compare the average column
225 over the valid pixels to the average MAX-DOAS column around the overpass time.

Case 2: We recalculate the values of TROPOMI VCD_{tropo} selected in case 1, using the median of the MAX-DOAS seasonal vertical profile according to Eq. (1) and Eq. (2) following Dimitropoulou et al. (2020). This recalculation is necessary to account for the different vertical sensitivity and a priori profile shapes of the TROPOMI and MAX-DOAS retrievals.

$$VCD_{MAX-DOAS}^{smoothed} = \sum_i AVK_i^{SP5} * C_{me}^{MAX-DOAS} \quad (1)$$

230 $VCD_{SP5}^{recal} = VCD_{SP5} * \frac{VCD_{MAX-DOAS}}{VCD_{MAX-DOAS}^{smoothed}} \quad (2)$

where $VCD_{MAX-DOAS}^{smoothed}$ represents the smoothed MAX-DOAS columns, AVK^{SP5} are the averaging Kernel of TROPOMI, $C_{me}^{MAX-DOAS}$ are the median profiles of the MAX-DOAS (in partial columns) discussed further below. We use the daily median profiles of MAX-DOAS to perform these transformations, in accordance with Dimitropoulou et al. (2020).^{Add} and^{Del} VCD_{SP5}^{recal} is the recalculated TROPOMI column using the MAX-DOAS profile as a priori. The index i denotes summation on the different
235 layers. ~~The median profiles used in this transformation are shown in Figure C1.~~^{Del}

Case 3: We proceed as in the previous case, but select only the pixels that lie in the azimuth direction of the instrument (355°). Previous studies have used this approach, exploiting the availability of measurements in different azimuth directions (Chen et al., 2009; Irie et al., 2008; Ma et al., 2013; Dimitropoulou et al., 2020). We then apply the transformation of case 2 to these selected pixels. The selection of TROPOMI pixels in the MAX-DOAS viewing direction is performed in
240 three steps illustrated on Fig. 5. First, a horizontal profile (0 to 10 km) is created, consisting of 20 equally spaced points (distance 0.5 km), starting from UniKin (4.42° S, 15.31° E) and oriented in the viewing direction of the instrument (355°). Second, geographical coordinates are assigned to each of the points. Finally, among the pixels lying within 20km of the observation site (24 in Fig. 5 a), only a few pixels cross the created line (3 pixels in Fig. 5b). Those are the pixels selected for the test within the MAX-DOAS line of sight.^{Add}

245 ~~The selection of TROPOMI pixels in the MAX-DOAS viewing direction is performed by creating a horizontal profile from 0 to 15km in 500 m steps starting from UniKin. The horizontal profile created is oriented in the viewing direction (355°). For each selected day, a coincidence test is performed between the TROPOMI pixels of the selected day and the points of the profile. The pixels whose surface point coincides with one of the points of our horizontal profile is selected.~~^{Del}

250 In all three studied cases, the selected MAX-DOAS measurements are hourly averages at the overpass time.^{Add} ~~For all three cases tested, the MAX-DOAS measurements are selected within a time interval of 1h around the TROPOMI satellite overpass.~~^{Del} Numerical results of daily and monthly averages are also presented for each case. Absolute ^{Add} median differences (SAT-GB expressed in 10^{15} molecules cm^{-2}), relative ^{Add} median differences (SAT-GB)/GB, in (%), and ^{Add} least-squares linear

255 regression statistics were calculated for each case. The results obtained for NO₂ and H₂CO are summarized ~~below~~^{Del} in Sect. 3.2.^{Add}

Figure 6 illustrates the daily median retrieved MAX-DOAS profiles (green dots) of NO₂ and H₂CO ~~for each season.~~^{Del} for 8 June and 15 November 2020, one day in the dry season and one day in the rainy season, respectively.^{Add} The daily median profile of TM5 and GEOS-Chem for each molecule (orange dots)^{Add} is also shown for these two days^{Add} ~~for each season.~~^{Del}. TM5 is a global chemistry transport model that is used to derive vertical profiles of NO₂ and H₂CO in TROPOMI product
260 retrievals with a horizontal resolution of 1° x 1° (Williams et al., 2017). The horizontal bars represent the standard deviations related to each case. On panel a, the NO₂ profiles recovered by MAX-DOAS are found to be reasonably close to those of the two models. This behaviour is typical of all MAX-DOAS daily median NO₂ profiles during the dry season (see Fig. C1). The MAX-DOAS profile seems to fit fairly well with the TM5 and GEOS-Chem profiles for the dry season. However, during the rainy season, on panel c, as on all the other days (see Fig. C1), both models underestimate the MAX-DOAS profile for
265 all altitudes. Regarding H₂CO, TM5 is found to overestimate the MAX-DOAS profile in the wet season. Most importantly, the TM5 profile during both seasons shows a fairly significant contribution in the upper troposphere, above 3 km, not found in the MAX-DOAS profile (see Fig. C1). This large difference in vertical profile can seriously impact the recalculation of TROPOMI columns performed in case 2 and have impact the comparisons presented in Section 3.2.^{Add} ~~The NO₂ profiles recovered by MAX-DOAS are close to those of TM5 with slight differences in intensity near the ground, between 500 and
270 3000 meters altitude for all 3 periods. At these altitudes, we see that the TM5 profile intensity presents lower values than those of MAX-DOAS, of the order of 1×10^{10} molecules cm⁻³ difference between the two.~~^{Del} For H₂CO, the TM5 profile pattern approaches that of MAX-DOAS only for the periods from October to April, thus the combination of the long rainy season and the short dry season. As for NO₂, in this period, we note that the intensity of the TM5 profiles remains lower than that of MAX-DOAS, with differences of about 1×10^{10} molecules cm⁻³ in this period. During the long dry season (May-Sept), the
275 TM5 profile shows a different pattern than MAX-DOAS. We note an increase in intensity between 1000 and 2000 m while at these altitudes, the MAX-DOAS profile decreases at a decreasing exponential rate. Between 500 and 1000 m, we also note that the intensity of the TM5 profile is lower than that of the MAX-DOAS, in the order of about 2×10^{10} molecules cm⁻³. These differences between the TM5 and MAX-DOAS Profiles motivate the application of the transformation presented in Case 2, the results of which are described in the next section.^{Del}

280 3 Results

The following section provides a description of the MAX-DOAS database of NO₂ and H₂CO VCD_{tropo} and Aerosols Optical Depth (AOD) and presents the results of comparisons made between model and satellite. In Sect. 3.1, we show the tropospheric columns and AODs time-series and the trace gases diurnal and seasonal variations. In Sect. 3.2, we present the MAX-DOAS and TROPOMI comparisons ~~and in Sect. 3.3 the GEOS-Chem vs TROPOMI results.~~^{Del} according to the three cases described
285 in Sect. 2.5.^{Add}

3.1 Overview of^{Add} the MAX-DOAS database

Figure 7~~Figure 4~~^{Del} shows the VCD_{tropo} of NO_2 and H_2CO (panels b, d) and the AOD (panels a, c). In each panel, the red curve represents the monthly average of the geophysical quantity displayed while the other curve connects the daily averages. AOD is retrieved in the visible (477 nm : panel a) and in ultraviolet (360 nm : panel c). The absence of measurements in ~~December~~
290 ~~2020~~^{Del} ~~November~~ ~~2020~~^{Add} is due to a technical problem. The other gaps visible especially in panel c and d for H_2CO and AOD are due to data removed from our database, not having satisfied the MMF selection criteria.

During the study period, the daily averages of the tropospheric vertical NO_2 columns vary between 1.3×10^{15} and ~~14.8~~^{Del} ~~11.8~~^{Add} $\times 10^{15}$ molecules cm^{-2} while the tropospheric vertical H_2CO columns range vary between 3.5×10^{15} molecules cm^{-2} and ~~26~~^{Del} ~~31~~^{Add} $\times 10^{15}$ molecules cm^{-2} . ~~The seasonal cycles of the monthly NO_2 and H_2CO VCD_{tropo} , show higher~~
295 ~~values during the dry seasons.~~^{Del} ~~With higher values measured during the dry seasons.~~^{Add}

The AOD daily averages observed at 360 nm vary between 0.1 and ~~1.3~~^{Del} ~~2.9~~^{Add} and are generally higher than the AOD observed at 477 nm varying between 0.1 and ~~0.9~~^{Del} ~~2.2~~^{Add}, due to increased scattering by aerosols at short wavelengths. Larger AOD values are also observed during the dry season, as for NO_2 and H_2CO , as illustrated by the decrease in visibility shown in Fig. 1 (panels a, b). This AOD increase can be explained by the accumulation of dust in the atmosphere over Kinshasa in the
300 dry season due to the lack of cleaning effect of precipitation. This increase of AOD during the dry season is also confirmed by the Moderate Resolution Imaging Spectroradiometer (MODIS) AOD measurements, ~~added with black lines in~~^{Del}. Figure D1 providing a good ~~There is a good~~^{Del} correspondence between the MODIS AODs at 550nm and those of MAX-DOAS observed at 477 nm.

Figure 8~~Figure 5~~^{Del} shows the mean diurnal variations of NO_2 and H_2CO VCD_{tropo} ~~for the full measurement period~~^{Del},
305 ~~calculated for all ground-based (GB) measurements around the overpass time (10-14h).~~^{Add} ~~,as observed from the ground (blue dots) and from space by TROPOMI (black dots). Error bars are the one-sigma standard deviations.~~^{Del} Three different periods are shown in these figures. The first period, from 1 January to 14 May, covers the short dry season, characterised by little rainfall. The second period, from 15 May to 14 September, covers the long dry season, when there is virtually no rainfall. The third period runs from 15 September to 31 December, covering the long rainy season.^{Add} ~~Note that the wet season from~~
310 ~~September to 15 May has been split into two periods. The first period runs from later September to December and the second from January to April. The second period is often called "short dry season" by the local community due to the small decrease in rainfall frequency during this period in comparison to the first period. The first obvious feature is the systematic difference between the ground-based observations compared to those of TROPOMI, during the whole period, for both molecules.~~^{Del}

Regarding NO_2 VCD_{tropo} , we note a weak diurnal increase of similar amplitude during the 3 periods mentioned above. In
315 the case of H_2CO VCD_{tropo} , the diurnal variation (also similar during the 3 periods) seems to be characterised by a maximum around noon in good agreement with Stavrakou et al. (2015)^{Add}. ~~This behavior could be related to the diurnal fires pattern, with most of the emissions around noon (70%) and 13:00~~^{Del} This behavior could be related to the diurnal pattern of biogenic emissions and fires. Isoprene emissions are favored by light and warm conditions (Guenther et al., 2006). Most of the fires occur around noon (70%) and 13:00^{Add} (22%), as reported by Cizungu et al. (2021) at the Luki Biosphere Reserve (5.5° N,

320 13.3° E), close to Kinshasa. The warmer and drier weather from noon onward is favoring the occurrence of fires and their spread. This would affect the H₂CO production with some delay, due to the VOCs oxidation. Oxidation of biogenic VOCs such as isoprene and monoterpenes leads to H₂CO typically after a few hours (Marais et al., 2012). For pyrogenic VOCs, their lifetime is highly variable, from a few hours to several days (Stavrakou et al., 2009).^{Add}

3.2 Intercomparison MAX-DOAS versus TROPOMI^{Add}

325 Table 3 summarizes the results from the comparisons in three cases. The direct comparisons between TROPOMI ~~pixels~~^{Del} and MAX-DOAS observations (case 1, see Fig. 9 ~~in the appendix~~^{Del}) yields poor agreement. We note low slopes (*s*) of ~~0.26~~^{Del} ~~0.18~~^{Add} and ~~0.89~~^{Del} ~~0.67~~^{Add} for the daily and monthly comparisons, respectively, and correlation coefficients (*R*) of ~~0.41~~^{Del} ~~0.32~~^{Add} and ~~0.83~~^{Del} ~~0.71~~^{Add}. The corresponding intercepts are large, in the order of ~~-1.15~~^{Del} ~~-1.26~~^{Add} × 10¹⁵ molecules cm⁻² (daily) and ~~-1.06~~^{Del} ~~-0.21~~^{Add} × 10¹⁵ molecules cm⁻² (monthly), showing a strong contribution of the additive component.

330 High negative median bias are also associated with these results, of the order of ~~-1.45~~^{Del} ~~-1.26~~^{Add} × 10¹⁵ molecules cm⁻² ~~-39.53%~~^{Del} ~~(-37.57%)~~^{Add} and ~~-1.02~~^{Del} ~~-1.69~~^{Add} × 10¹⁵ molecules cm⁻² ~~-40.47%~~^{Del} ~~(-39.16%)~~^{Add} for the daily and monthly comparisons, showing a strong underestimation of the TROPOMI observations relative to the MAX-DOAS observations. It should be noted that similar results were obtained using zenith measurements at the same site for NO₂ (Yombo Phaka et al., 2021). An underestimation of TROPOMI NO₂ observations was also frequently reported over large cities, e.g. by Griffin et al.

335 (2019); Ialongo et al. (2020); Zhao et al. (2020); Marais et al. (2021); Cai et al. (2022); Verhoelst et al. (2021) using NDACC ZSL-DOAS, MAX-DOAS and Pandonia global networks.

Moving to case 2, results are improved by making use of the MAX-DOAS profile shape information. Despite the relatively similar profile shapes of TM5 and MAX-DOAS (Fig. 6a, Fig. C1b^{Add}), the impact of using the MAX-DOAS profiles as a priori in TROPOMI column retrieval appears to be significant. The agreement between the two data sets improves considerably compared to the first case, particularly in terms of reducing the median difference, while the slopes and correlation coefficients have maintained nearly identical values. We find a ^{Add} ~~with~~^{Del} slope of ~~0.72~~^{Del} ~~0.21~~^{Add} and ~~0.87~~^{Del} ~~0.64~~^{Add} for daily and monthly comparisons respectively, and with correlation coefficients of ~~0.74~~^{Del} ~~0.30~~^{Add} and ~~0.80~~^{Del} ~~0.68~~^{Add} (see Fig. 10 ~~Fig. A2 in the appendix~~^{Del}). On the other hand, ~~negative~~^{Del} there is high additive component at the intercept, ^{Add} ~~intercepts~~^{Del} ~~of~~^{Del} ~~-0.23~~^{Del} ~~2.76~~^{Add} × 10¹⁵ molecules cm⁻² and ~~-0.52~~^{Del} ~~1.15~~^{Add} × 10¹⁵ molecules cm⁻² ~~is noted~~^{Add} for the daily and

345 monthly comparisons. Negative median bias are also associated with these results, of the order of ~~-1.20~~^{Del} ~~-0.09~~^{Add} × 10¹⁵ molecules cm⁻² ~~-34.95%~~^{Del} ~~(-2.33%)~~^{Add} and ~~-1.02~~^{Del} ~~-0.39~~^{Add} × 10¹⁵ molecules cm⁻² ~~-27.84%~~^{Del} ~~(-11.49%)~~^{Add} for the daily and monthly comparisons, respectively. These results show the large impact of the a priori in the TROPOMI validation process and confirms results from previous studies (e.g. Dimitropoulou et al. (2020)).

The comparison in case 3, for which only TROPOMI pixels lying in the MAX-DOAS viewing direction are selected is

350 the most complex approach, since it takes into account the ground-based observation direction and the impact of the a priori profile shape on the TROPOMI retrieval (see Fig. A1 ~~Fig. 7~~^{Del} in the appendix^{Add}). Although this case is potentially more realistic than case 2, as it addresses the spatial heterogeneity of the target compound in a more refined way, it implies a sharp reduction of the number of points making up the comparison sample. The number of TROPOMI data used for each co-location

with MAX-DOAS measurements is reduced by about a factor of 0.15 on average (see Fig. 5), in comparison with case 2. The number of days with valid data is also reduced from 198 to 90. Therefore, given the strong noise in the TROPOMI column data, the regression of case 3 should be considered with caution. Furthermore, as seen on Fig. 4, the NO₂ field shows a steep gradient along the line of sight between UniKin and a distance of 10 km. The case 3 assumes a uniform sensitivity of MAX-DOAS along the 10 km of the line of sight, even though the instrument is likely more sensitive to shorter distances, where NO₂ columns are lower. We note an increase relative to case 2, of the TROPOMI bias to around 40% for daily and monthly comparisons.^{Add} The possible causes explaining these differences are discussed in section 4. ~~Figure A1 Fig. B presents the results for this case. Figure A1a Fig. 8 shows the comparison of NO₂ daily MAX-DOAS (green dots) and TROPOMI (black dots) VCD_{tropo} from November 2019 to July 2021. We note a good agreement between the two data sets with a slope of 1.09, a correlation coefficient R=0.59, associated with a low bias of -1.56% for daily averages and for monthly averages (s=1.48; R=0.82 and a bias = -0.28%).^{Del}~~

Table 4 presents the results summary for H₂CO. As for NO₂, the direct comparison (case 1) shows poor agreement between TROPOMI and MAX-DOAS and the impact of a priori is also strongly visible in our comparisons for H₂CO. From the first (Fig. 11) to the second case (Fig. 12 in the appendix), there is a statistical improvement between TROPOMI and MAX-DOAS. The slopes and coefficients improve strongly when comparing daily averages (s= 0.26 to 0.72 and R= 0.41 to 0.74). The median biases associated with the results of these two cases from -4.90×10^{15} molecules cm⁻² (-26.12%) to -24% (-3.8×10^{15} molecules cm⁻² (1%) for the daily comparisons and from -4.99×10^{15} molecules cm⁻² (-28.89%) to -0.90×10^{15} molecules cm⁻² (-3.82%) for the monthly comparisons.^{Del}

Table 4 summarizes the results summary for H₂CO. As for NO₂, the direct comparison (case 1: Fig. 11 in appendix^{Del}) shows a strong median between TROPOMI and MAX-DOAS of around -5.91×10^{15} (-39%) (s=0.26, R = 0.43) for daily averages and -6.00×10^{15} (-39%) (s=0.68, R = 0.79) for monthly averages. TROPOMI is therefore underestimated.^{Add} These results (daily comparisons)^{Add} are close to those ~~consistent with^{Del}~~ presented in De Smedt et al. (2021), for the polluted sites of UNAM in Mexico and Xianghe in China. We also note an underestimation of TROPOMI compared to the ground measurements (~~case 1^{Del}~~), with H₂CO levels ranging from 1 to 25×10^{15} molecules cm⁻². Chan et al. (2020) and De Smedt et al. (2021) have also observed this underestimation in the case of large cities characterized by high pollution. The high H₂CO ~~VCD_{tropo}^{Del}~~ column levels (between 10 and 20×10^{15} molecules cm⁻² on monthly average)^{Add} characterize Kinshasa as a highly polluted ~~region^{Del}~~ area^{Add} (VCD_{tropo}^{Del} columns higher than 8×10^{15} molecules cm⁻²) ~~following^{Del}~~ according^{Add} to the methodology of Vigouroux et al. (2020), ~~that validated^{Del}~~ who validated^{Add} TROPOMI H₂CO using an extensive network of ground-based Fourier-transform infrared (FTIR) stations. In the same study, an average of 8.4 and 28×10^{15} molecules cm⁻² ~~are^{Del}~~ were^{Add} observed at the Paramaribo and Porto Velho stations, which are a highly polluted equatorial region in the same way as Kinshasa. Also in this study, we note a correlation coefficient of 0.8 between TROPOMI and the FTIR instrument of the Porto Velho station, value close to the one found in Kinshasa between TROPOMI and MAX-DOAS in case 2 (~~daily^{Del}~~ monthly^{Add} comparison).

For case 2 (Fig. 12), when taking the MAX-DOAS median profile as a priori, the median bias is highly reduced around 0.01×10^{15} (0.05%) (s=0.30, R = 0.20) for daily averages and 1.89×10^{15} molecules cm⁻² (11%) (s=1.00, R = 0.73) for monthly

averages. These results demonstrate the impact of applying the change of a priori as in the case of NO₂. Those results are in agreement with those of De Smedt et al. (2021), who found that the negative bias of TROPOMI H₂CO against MAX-DOAS data at highly polluted sites (Mexico City and Xianghe) was reduced when substituting the TM5 profiles with the MAX-DOAS profiles in the TROPOMI product. The effect was weaker for less polluted sites such as Uccle (De Smedt et al., 2021). In section 4, we investigate the possible causes of this significant decrease in bias.^{Add}

The third case (Fig. B1 Fig. 8^{Del} in the appendix), shows an improved agreement between the two datasets, despite a sharp reduction in the number of points included in the comparative sampling. Slopes and correlation coefficients are $s = 0.37$ and $R = 0.25$ for daily comparisons; $s=0.90$ and $R=0.55$ for monthly comparisons. The median bias is estimated at about 5% for both daily and monthly comparisons, which represents a strong improvement on case 2. We discuss these differences in section 4^{Add}

~~As for NO₂, the direct comparison (case 1) shows poor agreement between TROPOMI and MAX-DOAS and the impact of a priori is also strongly visible in our comparisons for H₂CO. From the first (Fig. 11 in the appendix) to the second case (Fig. 12 in the appendix), there is a statistical improvement between TROPOMI and MAX-DOAS. The slopes and coefficients improve strongly when comparing daily averages ($s=0.26$ to 0.72 and $R=0.41$ to 0.74). The median difference associated with the results of these two cases from -4.90×10^{15} molecules cm⁻² (-26.12%) to -0.24×10^{15} molecules cm⁻² (1%) for the daily comparisons and from -4.99×10^{15} molecules cm⁻² (-28.89%) to -0.90×10^{15} molecules cm⁻² (-3.82%) for the monthly comparisons.^{Del}~~

~~As for NO₂, the results of the third case are shown in Figure B1. Figure B1a shows the time series of daily comparisons for MAX-DOAS (green dots) and TROPOMI (black dots). The dynamic range of MAX-DOAS measurements is small compared to that of NO₂ because of the different points filtered according to the criteria described in Sect. 3.1 and because the H₂CO variability is quite different from the NO₂ one.^{Del}~~

~~In Figure B1a, the VCD_{tropo} of MAX-DOAS vary between 8.6 and 26.3×10^{15} molecules cm⁻². The corresponding statistics are presented in Figure B1b and d. Compared to case 2, there is a poorer agreement between the two data sets. This may be related to the reduced number of TROPOMI measurements involved in the averages, leading to poorer correlations ($R=0.60$ and $R=0.52$ respectively for comparisons between daily and monthly means). We note a strong reduction of about 70% of the number of pixels involved in the considered average. Positive median difference of 0.87×10^{15} molecules cm⁻² (13.40%) and 0.56×10^{15} molecules cm⁻² (17.05%) are found, respectively for comparisons based on daily and monthly averages, corresponding to an underestimation of MAX-DOAS data with respect to TROPOMI after application of the transformation.^{Del}~~

3.3 Intercomparison of GEOS-Chem with TROPOMI data sets^{Del}

The GEOS-Chem simulations used here cover the period from 1 January 2020 to 31 December 2020, and the mixing ratio profiles are produced at each 2h interval. We first performed a raw comparison between GEOS-Chem and TROPOMI, which showed that the model reasonably capture the temporal pattern of the NO₂ and H₂CO VCDs in the investigated area. Figure ?? presents this initial comparison.^{Del}

The output of the GEOS-Chem simulations were then regridded on the TROPOMI layering schemes and smoothed using the TROPOMI AVKs according to the formalism given in equation Eq. 3, as advised by Eskes et al. (2021).^{Del}

$$X_{\text{GEOS-Chem}}^{\text{smoothed}} = \sum_i AVK_i^{\text{SP5}} * X_g^{\text{Del}} \quad (3)$$

425 where $X_{\text{GEOS-Chem}}^{\text{smoothed}}$ represents the smoothed GEOS-Chem profile, AVK_{SP5} are the TROPOMI averaging Kernels and X_g^{Del} the regrided GEOS-Chem profile. An example of NO_2 and H_2CO sets profiles from the GEOS-Chem model are shown in Figure ?? . We note that the highest values of NO_2 and H_2CO are observed in the planetary boundary layer (PBL), below about 2 km above the surface between 8:00 and 10:00 am and in the evening from 4:00 pm. The lowest values of the near-surface concentration are observed between 10:00 and 14:00. These variations are primarily related to the daily variation of the height
430 of the boundary layer over the city of Kinshasa. We note strong increases of the BLH in the morning with a maximum reaching nearly 1300 m at sunrise and strong decreases at sunset (C3S, 2017). For comparisons between TROPOMI and GEOS-Chem, the model data are averaged +/- 1h around the overpass time (13h30 local time).^{Del}

Panels a and b from Figure ?? show the time series of daily and monthly averages respectively of TROPOMI (black dots) and GEOS-Chem model (red dots) simulations for NO_2 for 2020. TROPOMI data are averaged over the area of (3.05-5.02°S,
435 13.8-16.3°E) inline with the model resolution (2°x2.5°). Figure ??a indicates a good reproduction of NO_2 seasonal cycle by the GEOS-Chem model, as seen by TROPOMI. The highest NO_2 columns are observed during the dry season period (June-August), the period strongly affected by forest fires around Kinshasa (Cizungu et al., 2021). The linear regression between the two datasets, (Figure. ?? b, d) yields a good correlation between the two data sets, $R = 0.80$ for daily comparisons and $R = 0.96$ for monthly comparisons.^{Del} The regression slopes are of the order of 0.5, possibly suggesting an underestimation of
440 emissions during the dry season. We also note a small negative bias of about -0.32×10^{15} molecules cm^{-2} (-15.71%) related to the daily average and -0.37×10^{15} molecules cm^{-2} (-24.94%) related to sampling based on monthly averages.^{Del}

Figure ?? b, d showing the statistical results between the two H_2CO data sets, indicate a poor correlation between the two, with correlation coefficients of 0.24 and 0.67 for daily and monthly comparisons and low slopes of the order of 0.05 and 0.24 respectively. Compared to the NO_2 case, we find that for H_2CO there is a very poor linear correlation between the two data sets,
445 we simply observe a small bias between TROPOMI and the GEOS-Chem model (10%: monthly comparisons). We discuss the possible causes of this finding in Section 4.1^{Del}

4 Discussion

In this subsection, we present some elements that can explain the differences observed between the TROPOMI and MAX-DOAS and GEOS-Chem.^{Del} To this purpose, we focus on probing some of the physico-chemical parameters used in the different
450 inversion algorithms of these two datasets and we will also look at other independent parameters, specific to each dataset and the observation site.^{Del}

The main conclusions of the comparisons between TROPOMI and MAX-DOAS data are as follows. First, there is a general underestimation of TROPOMI NO_2 and H_2CO columns in comparison to the ground-based observations, when the differences

in vertical sensitivity and a priori profile shapes are not taken into account. Once those are considered in the comparison, there is a substantial improvement of the comparison statistics, especially, a strong impact on the reduction of the median difference between TROPOMI and MAX-DOAS^{Add}. The comparison using selected TROPOMI pixels along the line of sight of the MAX-DOAS instrument shows a substantial increase in the TROPOMI averages, especially for NO₂, in line with the strong heterogeneity of the target compounds shown on Fig. 4. However, this approach is more strongly affected by the TROPOMI noise, and likely overestimates the influence of the very polluted city center, located 5-10 km from the station^{Add}.
455
460 ~~Moreover, for NO₂ there is a clear improvement of the results when considering only TROPOMI pixel along the line of sight of the MAX-DOAS instrument. For H₂CO this is less obvious, probably due to the strong reduction of the number of pixels considered in the daily comparisons and the number of common days (102 instead of 208).~~^{Del}

The general underestimation of TROPOMI compared to MAX-DOAS observations (case 1)^{Add}, can be partly understood by the limitation of nadir-viewing satellites to capture the high pollution lying near the ground (averaging kernels often below one for the first kilometers close to the ground), as is often the case in large cities. Kinshasa and its surroundings, with its high population density, intense road traffic and the common use of embers from wood burnt in the forest, is highly polluted. Figure. 4 shows elevated concentrations of both molecules in downtown Kinshasa, located to the north of the measuring station, aligned with the viewing direction of the instrument. The southern part of the 20 km radius around the site is less polluted than the northern part, which may contribute to the underestimation of TROPOMI column averages in this radius. Furthermore, satellite retrieval heavily relies on choices made for the a priori profile. The a priori profile used in the inversion of the initial TROPOMI product is based the TM5 global model, featuring coarse horizontal resolution of 1° x 1° (Williams et al., 2017), which contrasts the fine horizontal resolution of TROPOMI (3.5×5.5 km²) and leads to biased comparisons. Accounting for sensitivity through TROPOMI averaging kernels in conjunction with the MAX-DOAS profile (case 2) allowed us to deduce a correction factor. This factor is employed to update the initial TROPOMI product and notably mitigate the bias between TROPOMI and MAX-DOAS. The correction has a significantly more noticeable impact on H₂CO compared to NO₂. This difference is attributed to the weaker vertical sensitivity near the surface in the UV range (H₂CO) as opposed to the Visible range (NO₂). Consequently, the influence of MAX-DOAS profiles is more substantial for H₂CO than for NO₂.^{Add}
465
470
475

~~The averaged satellite observations of NO₂ and H₂CO shown in Fig. 4 and present maximum values of 5×10^{15} molecules cm⁻² and 16.0×10^{15} molecules cm⁻² for NO₂ and H₂CO respectively. The satellite retrieval is thus greatly dependent on the choices made for its a priori profile. The low sensitivity of TROPOMI in the first layers near the surface is where the MAX-DOAS is the most sensitive, as shown in Fig. 3. Therefore, by taking into account the sensitivity via the TROPOMI AVKs, coupled to the MAX-DOAS profile (case 2), we were able to deduce a correction factor, which is used to transform the initial TROPOMI product. The results are improved compared to the initial comparison of case 1. It should also be noted that in the inversion of the original product TROPOMI, the a priori used is the one simulated by the TM5 model which is a global model with a large horizontal resolution of 1° x 1° (Williams et al., 2017) which remains coarse in comparison to the fine TROPOMI horizontal resolution (3.5×5.5 km²) thus leading to biased comparisons.~~^{Del}
480
485

Additional uncertainties comes from clouds and aerosols present practically the whole year in this region, affecting the accuracy of the satellite retrievals in the troposphere (e.g., Boersma et al., 2004; Koelemeijer et al., 2001; Heckel et al., 2011;

Leitão et al., 2010; McLinden et al., 2014). As seen in Fig. 7, AOD values can reach values up to 3 in the dry season. Although
490 the TROPOMI dataset selected in our study has been filtered to remove the high cloudiness scenes ($QA \geq 0.75$ for NO_2 and $QA \geq 0.5$ for H_2CO), it should be noted that this filtering does not totally eliminate all the scenes affected by clouds and aerosols. Lorente et al. (2017) estimates that the a priori, combined with the surface albedo and cloud parameters can lead to uncertainties of up to 47 % in the inversion of the TROPOMI data sets.

Considering only TROPOMI pixels intersecting the MAX-DOAS view (case 3) leads to elevated VCDs due to spatial
495 variation of NO_2 and H_2CO around Kinshasa. The northward-oriented pixels (Fig. 4) show higher concentrations, further amplified by applying transformation (1), explaining pronounced NO_2 biases. MAX-DOAS observations are heavily impacted by visibility, notably in Kinshasa with strong aerosol influence, reducing effective horizontal probing distance. This contributes to lower MAX-DOAS VCDs in case 3. Reduced pixel count (Figure 5) also diminishes statistical data points, adding to TROPOMI sampling noise.^{Add}

500 The increase in VCDs The improved agreement between TROPOMI and MAX-DOAS when considering only the TROPOMI pixels intersecting the MAX-DOAS field of view (case 3) can be understood in light of the horizontal variability of NO_2 and H_2CO around Kinshasa. Figure 4 illustrates the mean distributions of NO_2 and H_2CO columns at 0.01° resolution obtained by temporal oversampling of TROPOMI data during the study period. From Figure 4 these two figures, higher abundances are seen for both molecules in the city center of Kinshasa, which lies to the North of the measuring station, i.e. in the viewing
505 direction of the instrument. The southern part of the 20km-radius area defined around the site is less polluted than the northern part, which may partly explain the underestimation of TROPOMI NO_2 column averaged within a radius of 20km. By selecting only pixels lying in the pointing direction of the MAX-DOAS instrument, i.e. towards the North, the TROPOMI average reflects better the NO_2 levels sampled by the instrument and applying the transformation (1), this effect of increasing VCDs becomes even more dominant, justifying the high biases observed for NO_2 . It is pertinent to note that the MAX-DOAS observations are
510 significantly influenced by visibility. In the context of Kinshasa, which is greatly impacted by aerosols, the optical paths are reduced due to aerosol presence, thereby limiting the horizontal sensitivity to air masses near the instrument. From a statistical standpoint, a marked reduction in data points is also observed, which introduces noise into the TROPOMI sampling.^{Del}

4.1 Differences between GEOS-Chem and TROPOMI^{Del}

The difference in results between TROPOMI and the GEOS-Chem model may be due to several factors as the implemented
515 selected emission inventories, model chemistry involving the molecules studied and meteorological conditions, as well as the systematic biases in TROPOMI (e.g., Marais et al., 2021). The raw comparison between the satellite and model presented in Fig. ?? nevertheless gives confidence in the model outputs.^{Del}

The emission inventories used have finer resolutions than the model. Emission inventories such as DICE Africa and GFED have a spatial resolution of $0.1^\circ \times 0.1^\circ$, followed by RETRO: $0.25^\circ \times 0.25^\circ$, EDGAR: $0.5^\circ \times 0.5^\circ$, while the spatial resolution of
520 the model is $2^\circ \times 2.5^\circ$. This coarse spatial resolution can therefore affect the GEOS-Chem products and to diluting the emissions into a somewhat large box. Pan et al. (2020) indicates that aerosols from biomass burning emissions are poorly defined in global and regional models, with the impact of increasing uncertainties in understanding their impacts. The weather field is one of the

parameters that can also lead to uncertainties in the model. GEOS-Chem uses MERRA-2 with a coarse resolution of about 50 km in latitudinal direction. The comparative study of Jourdiere (2020), although conducted in the northern hemisphere (France),
525 on the evaluation of some weather fields including MERRA-2 to simulate wind speed, shows that MERRA-2 has high biases and overestimates wind speed, especially at night.^{Del}

5 Conclusions

We present the NO₂ and H₂CO MAX-DOAS measurements from an instrument installed at the University of Kinshasa in November 2019. Measurements in Africa are very scarce, and we use them in order to validate the TROPOMI tropospheric
530 columns^{Add}. ~~and evaluate the performance of the GEOS-Chem model^{Del}~~ This work complements the first DOAS NO₂ observations made in this region between 2017 and 2019. The ~~result^{Del} measurements^{Add}~~ obtained with the first instrument demonstrated a good agreement between TROPOMI and ground-based measurements, with a negative median bias of the order of -25% (Yombo Phaka et al., 2021). The present work aims at understanding and reducing the comparison bias by using the additional information provided by the new MAX-DOAS instrument (line-of-sight and retrieval of the gases vertical profiles).
535 Measurements from the MAX-DOAS instrument for the period from November 2019 to July 2021 were analyzed and inverted within the harmonized FRM4DOAS project facilities. The annual cycle of NO₂ and H₂CO present highest ~~VCDtropo values^{Del}~~ tropospheric column levels^{Add} during the dry season (mid-May to mid-September). The MAX-DOAS ~~VCDtropo values^{Del}~~ columns^{Add} of NO₂ varied between ~~1.8^{Del}1.3^{Add}~~ and ~~11^{Del}11.8^{Add}~~ × 10¹⁵ molecules cm⁻², while that of H₂CO varied between ~~5.4^{Del}3.5^{Add}~~ and ~~27^{Del}31^{Add}~~ × 10¹⁵ molecules cm⁻². These MAX-DOAS measurements are then compared
540 to the TROPOMI observations. ~~instrument on board the S5p satellite., for different comparison assumptions. In a second step, the TROPOMI observations are compared to simulations from the GEOS-Chem global model, over its 2° × 2.5° spatial resolution.^{Del}~~

The TROPOMI validation exercise was carried out following 3 steps: (1) a standard comparison involving an average of all pixels within a radius of 20 km around the observation site and an hourly average of VCD_{tr_op_o} MAX-DOAS at overpass
545 S5p^{Add} ~~average of VCD_{tr_op_o} MAX-DOAS (+/- 60 minutes) around the S5p overpass^{Del}~~, (2) recalculating the TROPOMI product using the MAX-DOAS profile as a priori, (3) selecting only the TROPOMI pixels within the MAX-DOAS line of sight and recalculating their VCD_{tr_op_o} as in the second case. The result of Case 1, complementing the previous exercise carried out at the same site, for NO₂, confirms that TROPOMI columns are underestimated, with a median bias of around -39%. When using the MAX-DOAS profile as a priori in the TROPOMI calculation, a significant improvement in the agreement between
550 the two datasets is observed. The differences between the two datasets are substantially reduced, about -2% ($s=0.21$, $R=0.30$) for daily averages and -12% ($s=0.64$, $R=0.68$) for monthly averages. For H₂CO, based on case1, we find a median bias of -39% ($s=0.26$, $R=0.43$) for daily averages and -39% ($s=0.68$, $R=0.79$) for monthly averages. In case 2, we find a strong bias reduction of around 0.05% ($s=0.30$, $R=0.20$) for averages and 11% ($s=1.00$, $R=0.73$) for monthly averages.^{Add}

~~The last case is^{Del}~~ The third case, although potentially more realistic as it optimizes the spatial overlap of the comparison (by
555 only selecting S5p pixels in the MAX-DOAS observation direction), shows less relevant statistical results than the other two,

due to the small sample size. Given the horizontal distribution of the two compounds, TROPOMI VCDs are very high in the direction of downtown Kinshasa, leading to strong biases in the comparison results.^{Add}

560 The comparison for case 3 shows a $s = 1.09$, $R = 0.59$ and bias = -1.6% for the daily comparison and $s = 1.48$, $R = 0.82$ and bias = -0.28% for comparisons between monthly means, for NO_2 . For H_2CO , we find a bias of 13% ($s = 1.51$ and $R = 0.6$) for the case 3 daily averages and 17% ($s = 1.78$ and $R = 0.52$) for monthly averages. The agreement between TROPOMI and MAX-DOAS H_2CO VCD_{tropo} is even better in the second case (1% and 4% biases), probably related to the larger number of comparisons points, reducing the noise on TROPOMI H_2CO . The present comparisons have shown the importance of correcting the initial TROPOMI products with the profile measured over the observation site.^{Del} and taking into account the horizontal variability of the studied molecules.^{Del}

565 Our study demonstrates and confirms the impact of using MAX-DOAS profiles as a priori in the retrieval of TROPOMI columns. Indeed, due to the satellite low sensitivity near the surface, biases can manifest significantly in conditions of highly polluted large cities like Kinshasa, potentially resulting in an underestimation of satellite observations. However, this tendency is markedly mitigated when correction is applied by considering profiles actually measured by the ground-based instrument.^{Add}

570 Consequently, our recommendation is to implement this transformation, particularly in settings of highly polluted urban areas like Kinshasa. Nonetheless, caution should be exercised in the incorporation of the MAX-DOAS line of sight due to the introduced noise during downsampling, as observed in this study.^{Add} This work also shows that the city of Kinshasa and its surroundings are very polluted in terms of NO_2 , H_2CO and aerosols, thus requiring regular monitoring and control by the leaders of the region.^{Del} authorities^{Add}.

575 We also tested the performance of the GEOS-Chem model to reproduce observations in this region. We performed some NO_2 and H_2CO simulations with the DICE-Africa anthropogenic emission inventory, the GFED biogenic and biomass fires inventory, and compared them with TROPOMI values.^{Del}

580 Because of the high spatial resolution of MAX-DOAS compared to the model, comparing the two make no sense. For NO_2 , the results of these comparisons showed a good agreement between TROPOMI and the model ($s = 0.42$, $R = 0.80$, bias = -15.71% for daily averages) and ($s = 0.51$, $R = 0.96$, bias = -24.94% for monthly averages). For H_2CO , the agreement is less good, with a bias of 61% ($s = 0.05$ and $R = 0.24$) for daily averages and 9.6% ($s = 0.24$ and $R = 0.67$) for monthly averages.^{Del}

Comparisons with the GEOS-Chem model have shown how well the emission inventories used are able to reproduce the TROPOMI observations over the Kinshasa region for NO_2 . For H_2CO further investigations on the emissions inventories are necessary to extend the work initiated in this study and find possible settings that improve the satellite-to-model comparison.^{Del}

585 *Data availability.* The spectra, DSCDs, profile and VCD supporting the conclusions of this study are available from BIRA-IASB. The GEOS-Chem data are available from ULiège. All these data are available upon request. Please contact the authors.

Author contributions. RYP participated in the installation of the instrument in Kinshasa, ran the simulations and processed the GEOS-Chem model data, developed the extraction algorithms and calculations for the comparison between TROPOMI versus MAX-DOAS and GEOS-Chem, and wrote the paper. AM and GP contributed to the design and installation of the MAX-DOAS instrument, extraction of FRM4DOAS products, provision of TROPOMI NO₂ data, scientific discussions, and editing of the paper. MMF and FH provided the FRM4DOAS tool for inversion of the MAX-DOAS data used, and guided RYP in understanding some of the concepts used. JFM and TS produced two TROPOMI oversampling figures, supported and guided RDY in interpreting the results, and participated actively in the scientific discussion. IDS provided the TROPOMI H₂CO data and participated in the scientific discussion. RBM and EPP participated in the scientific discussion. BLD is in charge of the MAX-DOAS instrument in Kinshasa. LJ participated in the design of the optical head of the instrument. CF and MVR have developed and made available to us QDOAS, have participated actively in scientific discussions. EM and JPM supervised the present work, provided general guidance and valuable comments throughout the process of preparing the paper, and reviewed and edited the paper. All authors reviewed, discussed, and commented on the article.

Competing interests. At least one of the (co-)authors is a member of the editorial board of Atmospheric Measurement Techniques. The peer-review process was guided by an independent editor, and the authors also have no other competing interests to declare.

Disclaimer. TEXT

Acknowledgements. We thank Robert Spurr for free deployment of VLIDORT. The MERRA-2 data used in this study have been provided by the Global Modeling and Assimilation Office (GMAO) at NASA Goddard Space Flight Center. We thank Claudio Queirolo for his valuable contribution in the realization of the few materials used in this work. We also thank Nuno Pereira for useful discussions and Professor Jacob Sabkinu for his support of our project. Rodriguez Yombo Phaka benefits from a scholarship funded by the Académie de Recherche et d'Enseignement Supérieur–Commission de la Coopération au Développement (ARES–CCD), managed at ULiège by the Centre pour le Partenariat et la Coopération au Développement (PACODEL). Emmanuel Mahieu is a senior research associate with the F.R.S.–FNRS. We thank Claudio Queirolo for his valuable contribution in the realization of the few materials used in this work. This research is partly supported by the Belgian Science Policy Office (BELSPO) through the EQUATOR (Emission Quantification of Atmospheric tracers in the Tropics using Observations from satellites) project 2021-2025.

References

- 610 Bauwens, M., Stavrou, T., Müller, J.-F., De Smedt, I., Van Roozendaal, M., van der Werf, G. R., Wiedinmyer, C., Kaiser, J. W., Sindelarova, K., and Guenther, A.: Nine years of global hydrocarbon emissions based on source inversion of OMI formaldehyde observations, *Atmospheric Chemistry and Physics*, 16, 10 133–10 158, <https://doi.org/10.5194/acp-16-10133-2016>, 2016.
- Beirle, S., Dörner, S., Donner, S., Remmers, J., Wang, Y., and Wagner, T.: The Mainz profile algorithm (MAPA), *Atmos. Meas. Tech.*, 12, 1785–1806, <https://doi.org/10.5194/amt-12-1785-2019>, 2019.
- 615 Bockarie, A. S., Marais, E. A., and MacKenzie, A. R.: Air Pollution and Climate Forcing of the Charcoal Industry in Africa, *Environmental Science & Technology*, 54, 13 429–13 438, <https://doi.org/10.1021/acs.est.0c03754>, 2020.
- Boersma, K. F., Eskes, H. J., and Brinkma, E. J.: Error analysis for tropospheric NO₂ retrieval from space, *Journal of Geophysical Research: Atmospheres*, 109, <https://doi.org/10.1029/2003jd003962>, 2004.
- Bogumil, K., Orphal, J., Homann, T., Voigt, S., Spietz, P., Fleischmann, O., Vogel, A., Hartmann, M., Kromminga, H., Bovensmann, H.,
- 620 Frerick, J., and Burrows, J.: Measurements of molecular absorption spectra with the SCIAMACHY pre-flight model: instrument characterization and reference data for atmospheric remote-sensing in the 230–2380 nm region, *Journal of Photochemistry and Photobiology A: Chemistry*, 157, 167–184, [https://doi.org/https://doi.org/10.1016/S1010-6030\(03\)00062-5](https://doi.org/https://doi.org/10.1016/S1010-6030(03)00062-5), atmospheric Photochemistry, 2003.
- C3S: ERA5: Fifth generation of ECMWF atmospheric reanalyses of the global climate. Copernicus Climate Change Service Climate Data Store (CDS), accessed 24 September 2019, 2017.
- 625 Cai, K., Li, S., Lai, J., Xia, Y., Wang, Y., Hu, X., and Li, A.: Evaluation of TROPOMI and OMI Tropospheric NO₂ Products Using Measurements from MAX-DOAS and State-Controlled Stations in the Jiangsu Province of China, *Atmosphere*, 13, 886, <https://doi.org/10.3390/atmos13060886>, 2022.
- Chan, K. L., Wiegner, M., Geffen, J. V., Smedt, I. D., Alberti, C., Cheng, Z., Ye, S., and Wenig, M.: MAX-DOAS measurements of tropospheric NO₂ and HCHO in Munich and the comparison to OMI and TROPOMI satellite observations, *Atmos. Meas. Tech.*, 13, 4499–4520,
- 630 <https://doi.org/10.5194/amt-13-4499-2020>, 2020.
- Chance, K. and Kurucz, R. L.: An improved high-resolution solar reference spectrum for earth's atmosphere measurements in the ultraviolet, visible, and near infrared, *Journal of Quantitative Spectroscopy and Radiative Transfer*, 111, 1289–1295, <https://doi.org/10.1016/j.jqsrt.2010.01.036>, 2010.
- Chance, K. V. and Spurr, R. J. D.: Ring effect studies: Rayleigh scattering, including molecular parameters for rotational Raman scattering, and the Fraunhofer spectrum, *Appl. Opt.*, 36, 5224, <https://doi.org/10.1364/ao.36.005224>, 1997.
- Chen, D., Zhou, B., Beirle, S., Chen, L. M., and Wagner, T.: Tropospheric NO₂ column densities deduced from zenith-sky DOAS measurements in Shanghai, China, and their application to satellite validation, *Atmos. Chem. Phys.*, 9, 3641–3662, <https://doi.org/10.5194/acp-9-3641-2009>, 2009.
- Cheng, Y., Wang, Y., Zhang, Y., Crawford, J. H., Diskin, G. S., Weinheimer, A. J., and Fried, A.: Estimator of Surface Ozone Using Formaldehyde and Carbon Monoxide Concentrations Over the Eastern United States in Summer, *Journal of Geophysical Research: Atmospheres*,
- 640 123, 7642–7655, <https://doi.org/https://doi.org/10.1029/2018JD028452>, 2018.
- Cizungu, N. C., Tshibusu, E., Lutete, E., Mushagalusa, C. A., Mugumaarhahama, Y., Ganza, D., Karume, K., Michel, B., Lumbuenamo, R., and Bogaert, J.: Fire risk assessment, spatiotemporal clustering and hotspot analysis in the Luki biosphere reserve region, western DR Congo, *Trees, Forests and People*, 5, 100 104, <https://doi.org/https://doi.org/10.1016/j.tfp.2021.100104>, 2021.

- 645 Crutzen, P. J.: The role of NO and NO₂ in the chemistry of the troposphere and stratosphere, *Ann. Rev. Earth Planet. Sci.*, 7, 443–72, www.annualreviews.org, 1979.
- Danckaert, T. and Fayt, C.: QDOAS Software user manual, September, Royal Belgian Institute for Space Aeronomy (BIRA), Brussel, 2017.
- de Foy, B., Krotkov, N. A., Bei, N., Herndon, S. C., Huey, L. G., Martínez, A.-P., Ruiz-Suárez, L. G., Wood, E. C., Zavala, M., and Molina, L. T.: Hit from both sides: tracking industrial and volcanic plumes in Mexico City with surface measurements and OMI SO₂ retrievals
650 during the MILAGRO field campaign, *Atmospheric Chemistry and Physics*, 9, 9599–9617, <https://doi.org/10.5194/acp-9-9599-2009>, 2009.
- De Smedt, I., Stavrou, T., Hendrick, F., Danckaert, T., Vlemmix, T., Pinardi, G., Theys, N., Lerot, C., Gielen, C., Vigouroux, C., Hermans, C., Fayt, C., Veefkind, P., Müller, J. F., and Van Roozendael, M.: Diurnal, seasonal and long-term variations of global formaldehyde columns inferred from combined OMI and GOME-2 observations, *Atmos. Chem. Phys.*, 15, 12 519–12 545, <https://doi.org/10.5194/acp-15-12519-2015>, 2015.
655
- De Smedt, I., Pinardi, G., Vigouroux, C., Compernelle, S., Bais, A., Benavent, N., Boersma, F., Chan, K. L., Donner, S., Eichmann, K. U., Hedelt, P., Hendrick, F., Irie, H., Kumar, V., Lambert, J. C., Langerock, B., Lerot, C., Liu, C., Loyola, D., PETERS, A., Richter, A., Rivera Cárdenas, C., Romahn, F., Ryan, R. G., Sinha, V., Theys, N., Vlietinck, J., Wagner, T., Wang, T., Yu, H., and Van Roozendael, M.: Comparative assessment of TROPOMI and OMI formaldehyde observations and validation against MAX-DOAS network column measurements,
660 *Atmos. Chem. Phys.*, 21, 12 561–12 593, <https://doi.org/10.5194/acp-21-12561-2021>, 2021.
- Dimitropoulou, E., Hendrick, F., Pinardi, G., Friedrich, M. M., Merlaud, A., Tack, F., Longueville, H. D., Fayt, C., Hermans, C., Laffineur, Q., Fierens, F., and Roozendael, M. V.: Validation of TROPOMI tropospheric NO₂ columns using dual-scan multi-axis differential optical absorption spectroscopy (MAX-DOAS) measurements in Uccle, Brussels, *Atmos. Meas. Tech.*, 13, 5165–5191, <https://doi.org/10.5194/amt-13-5165-2020>, 2020.
- 665 Eskes, H., Geffen, J. V., Boersma, F., Eichmann, K.-U., Apituley, A., Pedernana, M., Sneep, M., Veefkind, J. P., and Loyola, D.: Sentinel-5 precursor/TROPOMI Level 2 Product User Manual Nitrogen dioxide document number : S5P-KNMI-L2-0021-MA, 2021.
- Fleischmann, O. C., Hartmann, M., Burrows, J. P., and Orphal, J.: New ultraviolet absorption cross-sections of BrO at atmospheric temperatures measured by time-windowing Fourier transform spectroscopy, *Journal of Photochemistry and Photobiology A: Chemistry*, 168, 117–132, <https://doi.org/https://doi.org/10.1016/j.jphotochem.2004.03.026>, 2004.
- 670 Fortems-Cheiney, A., Chevallier, F., Pison, I., Bousquet, P., Saunois, M., Szopa, S., Cressot, C., Kurosu, T. P., Chance, K., and Fried, A.: The formaldehyde budget as seen by a global-scale multi-constraint and multi-species inversion system, *Atmospheric Chemistry and Physics*, 12, 6699–6721, <https://doi.org/10.5194/acp-12-6699-2012>, 2012.
- Friedrich, M., Rivera, C., Stremme, W., Ojeda, Z., Arellano, J., Bezanilla, A., García-Reynoso, J. A., and Grutter, M.: NO₂ vertical profiles and column densities from MAX-DOAS measurements in Mexico City, *Atmos. Meas. Tech.*, 12, 2545–2565, <https://doi.org/10.5194/amt-12-2545-2019>, 2019.
675
- Frieß, U., Beirle, S., Alvarado Bonilla, L., Bösch, T., Friedrich, M. M., Hendrick, F., PETERS, A., Richter, A., van Roozendael, M., Rozanov, V. V., Spinei, E., Tirpitz, J.-L., Vlemmix, T., Wagner, T., and Wang, Y.: Intercomparison of MAX-DOAS vertical profile retrieval algorithms: studies using synthetic data, *Atmos. Meas. Tech.*, 12, 2155–2181, <https://doi.org/10.5194/amt-12-2155-2019>, 2019.
- FRM4DOAS ATBD, A.: Fiducial Reference Measurements for Ground-Based DOAS Air-Quality Observations Deliverable D3 : MAX-DOAS Instruments Review, Tech. Rep. 4000118181, 2017.
680

- Gielen, C., Roozendaal, M. V., Hendrick, F., Pinardi, G., Vlemmix, T., Bock, V. D., Backer, H. D., Fayt, C., Hermans, C., Gillotay, D., and Wang, P.: A simple and versatile cloud-screening method for MAX-DOAS retrievals, *Atmos. Meas. Tech.*, 7, 3509–3527, <https://doi.org/10.5194/amt-7-3509-2014>, 2014.
- 685 Griffin, D., Zhao, X., McLinden, C. A., Boersma, F., Bourassa, A., Dammers, E., Degenstein, D., Eskes, H., Fehr, L., Fioletov, V., Hayden, K., Kharol, S. K., Li, S. M., Makar, P., Martin, R. V., Mihele, C., Mittermeier, R. L., Krotkov, N., Sneep, M., Lamsal, L. N., ter Linden, M., van Geffen, J., Veefkind, P., and Wolde, M.: High-Resolution Mapping of Nitrogen Dioxide With TROPOMI: First Results and Validation Over the Canadian Oil Sands, *Geophysical Research Letters*, 46, 1049–1060, <https://doi.org/10.1029/2018GL081095>, 2019.
- 690 Guenther, A., Karl, T., Harley, P., Wiedinmyer, C., Palmer, P. I., and Geron, C.: Estimates of global terrestrial isoprene emissions using MEGAN (Model of Emissions of Gases and Aerosols from Nature), *Atmospheric Chemistry and Physics*, 6, 3181–3210, <https://hal.science/hal-00295995>, 2006.
- Harder, J. W. and Brault, J. W.: Atmospheric measurements of water vapor in the 442-nm region, *Journal of Geophysical Research: Atmospheres*, 102, 6245–6252, <https://doi.org/https://doi.org/10.1029/96JD01730>, 1997.
- Heckel, A., Kim, S. W., Frost, G. J., Richter, A., Trainer, M., and Burrows, J. P.: Influence of low spatial resolution a priori data on tropospheric NO₂ satellite retrievals, *Atmos. Meas. Tech.*, 4, 1805–1820, <https://doi.org/10.5194/amt-4-1805-2011>, 2011.
- 695 Hermans, C., Vandaele, A. C., Fally, S., Carleer, M., Colin, R., Coquart, B., Jenouvrier, A., and Merienne, M.-F.: Absorption Cross-section of the Collision-Induced Bands of Oxygen from the UV to the NIR, in: *Weakly Interacting Molecular Pairs: Unconventional Absorbers of Radiation in the Atmosphere*, edited by Camy-Peyret, C. and Vigasin, A. A., pp. 193–202, Springer Netherlands, Dordrecht, 2003.
- Ialongo, I., Virta, H., Eskes, H., Hovila, J., and Douros, J.: Comparison of TROPOMI/Sentinel-5 Precursor NO₂ observations with ground-based measurements in Helsinki, *Atmos. Meas. Tech.*, 13, 205–218, <https://doi.org/10.5194/amt-13-205-2020>, 2020.
- 700 Irie, H., Kanaya, Y., Akimoto, H., Tanimoto, H., Wang, Z., Gleason, J. F., and Bucsele, E. J.: Validation of OMI tropospheric NO₂ column data using MAX-DOAS measurements deep inside the North China Plain in June 2006: Mount Tai Experiment 2006, *Atmospheric Chemistry and Physics*, 8, 6577–6586, <https://doi.org/10.5194/acp-8-6577-2008>, 2008.
- Jourdi er, B.: Evaluation of ERA5, MERRA-2, COSMO-REA6, NEWA and AROME to simulate wind power production over France, vol. 17, pp. 63–77, Copernicus GmbH, <https://doi.org/10.5194/asr-17-63-2020>, 2020.
- 705 Karagkiozidis, D., Friedrich, M. M., Beirle, S., Bais, A., Hendrick, F., Voudouri, K. A., Fountoulakis, I., Karanikolas, A., Tzoumaka, P., Van Roozendaal, M., Balis, D., and Wagner, T.: Retrieval of tropospheric aerosol, NO₂, and HCHO vertical profiles from MAX-DOAS observations over Thessaloniki, Greece: intercomparison and validation of two inversion algorithms, *Atmos. Meas. Tech.*, 15, 1269–1301, <https://doi.org/10.5194/amt-15-1269-2022>, 2022.
- Keller, C. A., Long, M. S., Yantosca, R. M., Da Silva, A. M., Pawson, S., and Jacob, D. J.: HEMCO v1.0: A versatile, ESMF-compliant component for calculating emissions in atmospheric models, *Geoscientific Model Development*, 7, 1409–1417, <https://doi.org/10.5194/gmd-7-1409-2014>, 2014.
- 710 Koelemeijer, R. B., Stammes, P., Hovenier, J. W., and Haan, J. F. D.: A fast method for retrieval of cloud parameters using oxygen a band measurements from the Global Ozone Monitoring Experiment, *Journal of Geophysical Research Atmospheres*, 106, 3475–3490, <https://doi.org/10.1029/2000JD900657>, 2001.
- 715 Leit ao, J., Richter, A., Vrekoussis, M., Kokhanovsky, A., Zhang, Q. J., Beekmann, M., and Burrows, J. P.: Atmos. Meas. Tech. On the improvement of NO₂ satellite retrievals-aerosol impact on the air mass factors, *Atmos. Meas. Tech.*, 3, 475–493, www.atmos-meas-tech.net/3/475/2010/, 2010.

- Lioussé, C., Assamoi, E., Criqui, P., Granier, C., and Rosset, R.: Explosive growth in African combustion emissions from 2005 to 2030, *Environ. Res. Lett.*, 9, <https://doi.org/10.1088/1748-9326/9/3/035003>, 2014.
- 720 Lorente, A., Boersma, K. F., Yu, H., Dörner, S., Hilboll, A., Richter, A., Liu, M., Lamsal, L. N., Barkley, M., Smedt, I. D., Roozendael, M. V., Wang, Y., Wagner, T., Beirle, S., Lin, J. T., Krotkov, N., Stammes, P., Wang, P., Eskes, H. J., and Krol, M.: Structural uncertainty in air mass factor calculation for NO₂ and HCHO satellite retrievals, *Atmos. Meas. Tech.*, 10, 759–782, <https://doi.org/10.5194/amt-10-759-2017>, 2017.
- Lunt, M., Palmer, P., Feng, L., Taylor, C., Boesch, H., and Parker, R.: An increase in methane emissions from tropical Africa between 2010
725 and 2016 inferred from satellite data, *Atmospheric Chemistry and Physics Discussions*, pp. 1–30, <https://doi.org/10.5194/acp-2019-477>, 2019.
- Ma, J. Z., Beirle, S., Jin, J. L., Shaiganfar, R., Yan, P., and Wagner, T.: Tropospheric NO₂ vertical column densities over Beijing: Results of the first three years of ground-based MAX-DOAS measurements (2008-2011) and satellite validation, *Atmos. Chem. Phys.*, 13, 1547–1567, <https://doi.org/10.5194/acp-13-1547-2013>, 2013.
- 730 Marais, E. A. and Wiedinmyer, C.: Air Quality Impact of Diffuse and Inefficient Combustion Emissions in Africa (DICE-Africa), *Environmental Science and Technology*, 50, 10 739–10 745, <https://doi.org/10.1021/acs.est.6b02602>, 2016.
- Marais, E. A., Jacob, D. J., Kurosu, T. P., Chance, K., Murphy, J. G., Reeves, C., Mills, G., Casadio, S., Millet, D. B., Barkley, M. P., Paulot, F., and Mao, J.: Isoprene emissions in Africa inferred from OMI observations of formaldehyde columns, *Atmospheric Chemistry and Physics*, 12, 6219–6235, <https://doi.org/10.5194/acp-12-6219-2012>, 2012.
- 735 Marais, E. A., Silvern, R. F., Vodonos, A., Dupin, E., Bockarie, A. S., Mickley, L. J., and Schwartz, J.: Air Quality and Health Impact of Future Fossil Fuel Use for Electricity Generation and Transport in Africa, *Environmental Science & Technology*, 53, 13 524–13 534, <https://doi.org/10.1021/acs.est.9b04958>, 2019.
- Marais, E. A., Roberts, J. F., Ryan, R. G., Eskes, H., Boersma, K. F., Choi, S., Joiner, J., Abuhassan, N., Redondas, A., Grutter, M., Cede, A., Gomez, L., and Navarro-Comas, M.: New observations of NO₂ in the upper troposphere from TROPOMI, *Atmos. Meas. Tech.*, 14,
740 2389–2408, <https://doi.org/10.5194/amt-14-2389-2021>, 2021.
- Mayaux, P., Pekel, J. F., Desclée, B., Donnay, F., Lupi, A., Achard, F., Clerici, M., Bodart, C., Brink, A., Nasi, R., and Belward, A.: State and evolution of the African rainforests between 1990 and 2010, *Philosophical Transactions of the Royal Society B: Biological Sciences*, 368, <https://doi.org/10.1098/rstb.2012.0300>, 2013.
- McFarlane, C., Isevlambire, P. K., Lumbuenamo, R. S., Ndinga, A. M. E., Dhammapala, R., Jin, X., McNeill, V. F., Malings, C., Subramanian, R., and Westervelt, D. M.: First measurements of ambient pm_{2.5} in kinshasa, democratic republic of congo and brazzaville, republic
745 of congo using field-calibrated low-cost sensors, *Aerosol and Air Quality Research*, 21, <https://doi.org/10.4209/aaqr.200619>, 2021.
- McLinden, C. A., Fioletov, V., Boersma, K. F., Krotkov, N., Sioris, C. E., Veefkind, J. P., and Yang, K.: Air quality over the Canadian oil sands: A first assessment using satellite observations, *Geophysical Research Letters*, 39, <https://doi.org/https://doi.org/10.1029/2011GL050273>, 2012.
- 750 McLinden, C. A., Fioletov, V., Boersma, K. F., Kharol, S. K., Krotkov, N., Lamsal, L., Makar, P. A., Martin, R. V., Veefkind, J. P., and Yang, K.: Improved satellite retrievals of NO₂ and SO₂ over the Canadian oil sands and comparisons with surface measurements, *Atmos. Chem. Phys.*, 14, 3637–3656, <https://doi.org/10.5194/acp-14-3637-2014>, 2014.
- Meller, R. and Moortgat, G. K.: Temperature dependence of the absorption cross sections of formaldehyde between 223 and 323 K in the wavelength range 225-375 nm, *J. Geophys. Res. Atmos.*, 105, 7089–7101, <https://doi.org/10.1029/1999JD901074>, 2000.

- 755 Pan, X., Ichoku, C., Chin, M., Bian, H., Darmenov, A., Colarco, P., Ellison, L., Kucsera, T., Da Silva, A., Wang, J., Oda, T., and Cui, G.: Six global biomass burning emission datasets: Intercomparison and application in one global aerosol model, *Atmos. Chem. Phys.*, 20, 969–994, <https://doi.org/10.5194/acp-20-969-2020>, 2020.
- Pinardi, G., Van Roozendaal, M., Abuhassan, N., Adams, C., Cede, A., Clémer, K., Fayt, C., Frieß, U., Gil, M., Herman, J., Hermans, C., Hendrick, F., Irie, H., Merlaud, A., Navarro Comas, M., Peters, E., Piters, A. J. M., Puentedura, O., Richter, A., Schönhardt, A., Shaiganfar, R.,
- 760 Spinei, E., Strong, K., Takashima, H., Vrekoussis, M., Wagner, T., Wittrock, F., and Yilmaz, S.: MAX-DOAS formaldehyde slant column measurements during CINDI: intercomparison and analysis improvement, *Atmos. Meas. Tech.*, 6, 167–185, <https://doi.org/10.5194/amt-6-167-2013>, 2013.
- Pinardi, G., van Roozendaal, M., Hendrick, F., Theys, N., Abuhassan, N., Bais, A., Boersma, F., Cede, A., Chong, J., Donner, S., Drosoglou, T., Dzhola, A., Eskes, H., Frieß, U., Granville, J., Herman, J. R., Holla, R., Hovila, J., Irie, H., Kanaya, Y., Karagkiozidis, D., Kouremeti,
- 765 N., Lambert, J. C., Ma, J., Peters, E., Piters, A., Postlyakov, O., Richter, A., Remmers, J., Takashima, H., Tiefengraber, M., Valks, P., Vlemmix, T., Wagner, T., and Wittrock, F.: Validation of tropospheric NO₂ column measurements of GOME-2A and OMI using MAX-DOAS and direct sun network observations, *Atmos. Meas. Tech.*, 13, 6141–6174, <https://doi.org/10.5194/amt-13-6141-2020>, 2020.
- Poraicu, C., Müller, J.-F., Stavrou, T., Fonteyn, D., Tack, F., Deutsch, F., Laffineur, Q., Van Malderen, R., and Veldeman, N.: Cross-evaluating WRF-Chem v4.1.2, TROPOMI, APEX, and in situ NO₂ measurements over Antwerp, Belgium, *Geoscientific Model Development*,
- 770 16, 479–508, <https://doi.org/10.5194/gmd-16-479-2023>, 2023.
- Seinfeld, J. H. and Pandis, S. N.: *From Air Pollution to Climate Change*, Atmos. Chem. Phys. John Wiley and Sons, Inc, 1998.
- Serdyuchenko, A., Gorshelev, V., Weber, M., Chehade, W., and Burrows, J. P.: High spectral resolution ozone absorption cross-sections Part 2: Temperature dependence, *Atmos. Meas. Tech.*, 7, 625–636, <https://doi.org/10.5194/amt-7-625-2014>, 2014.
- Spurr, R.: *User 's Guide VLIDORT Version 2.6*, vol. 1183, RT Solutions, Inc., 2013.
- 775 Stavrou, T., Müller, J.-F., De Smedt, I., Van Roozendaal, M., van der Werf, G. R., Giglio, L., and Guenther, A.: Evaluating the performance of pyrogenic and biogenic emission inventories against one decade of space-based formaldehyde columns, *Atmospheric Chemistry and Physics*, 9, 1037–1060, <https://doi.org/10.5194/acp-9-1037-2009>, 2009.
- Stavrou, T., Müller, J.-F., Bauwens, M., De Smedt, I., Van Roozendaal, M., De Mazière, M., Vigouroux, C., Hendrick, F., George, M., Clerbaux, C., Coheur, P.-F., and Guenther, A.: How consistent are top-down hydrocarbon emissions based on formaldehyde observations
- 780 from GOME-2 and OMI?, *Atmospheric Chemistry and Physics*, 15, 11 861–11 884, <https://doi.org/10.5194/acp-15-11861-2015>, 2015.
- Tack, F., Merlaud, A., Iordache, M.-D., Pinardi, G., Dimitropoulou, E., Eskes, H., Bomans, B., Veefkind, P., and Roozendaal, M. V.: Assessment of the TROPOMI tropospheric NO₂ product based on airborne APEX observations, *Atmos. Meas. Tech.*, 14, 615–646, <https://doi.org/10.5194/amt-14-615-2021>, 2021.
- Thalman, R. and Volkamer, R.: Temperature dependent absorption cross-sections of O₂–O₂ collision pairs between 340 and 630 nm and at
- 785 atmospherically relevant pressure, *Phys. Chem. Chem. Phys.*, 15, 15 371–15 381, <https://doi.org/10.1039/C3CP50968K>, 2013.
- Tirpitz, J.-L., Frieß, U., Hendrick, F., Alberti, C., Allaart, M., Apituley, A., Bais, A., Beirle, S., Berkhout, S., Bogner, K., Bösch, T., Bruchkouski, I., Cede, A., Chan, K. L., den Hoed, M., Donner, S., Drosoglou, T., Fayt, C., Friedrich, M. M., Frumau, A., Gast, L., Gielen, C., Gomez-Martín, L., Hao, N., Hensen, A., Henzing, B., Hermans, C., Jin, J., Kreher, K., Kuhn, J., Lampel, J., Li, A., Liu, C., Liu, H., Ma, J., Merlaud, A., Peters, E., Pinardi, G., Piters, A., Platt, U., Puentedura, O., Richter, A., Schmitt, S., Spinei, E., Stein Zweers, D., Strong,
- 790 K., Swart, D., Tack, F., Tiefengraber, M., van der Hoff, R., van Roozendaal, M., Vlemmix, T., Vonk, J., Wagner, T., Wang, Y., Wang, Z., Wenig, M., Wiegner, M., Wittrock, F., Xie, P., Xing, C., Xu, J., Yela, M., Zhang, C., and Zhao, X.: Intercomparison of MAX-DOAS vertical

- profile retrieval algorithms: studies on field data from the CINDI-2 campaign, *Atmos. Meas. Tech.*, 14, 1–35, <https://doi.org/10.5194/amt-14-1-2021>, 2021.
- UN: The World's cities in 2016: data booklet, 2016.
- 795 van Geffen, J., Eskes, H., Compernelle, S., Pinardi, G., Verhoelst, T., Lambert, J.-C., Sneep, M., ter Linden, M., Ludewig, A., Boersma, K. F., and Veefkind, J. P.: Sentinel-5P TROPOMI NO₂ retrieval: impact of version v2.2 improvements and comparisons with OMI and ground-based data, *Atmospheric Measurement Techniques*, 15, 2037–2060, <https://doi.org/10.5194/amt-15-2037-2022>, 2022.
- Vandaele, A. C., Hermans, C., Simon, P. C., Carleer, M., Colin, R., Fally, S., Mérienne, M. F., Jenouvrier, A., and Coquart, B.: Measurements of the NO₂ absorption cross-section from 42 000 cm⁻¹ to 10 000 cm⁻¹ (238–1000 nm) at 220 K and 294 K, *J. Quant. Spectrosc. Radiat. Transf.*, 59, 171–184, [https://doi.org/10.1016/S0022-4073\(97\)00168-4](https://doi.org/10.1016/S0022-4073(97)00168-4), 1998.
- 800 Veefkind, J. P., Aben, I., McMullan, K., Förster, H., de Vries, J., Otter, G., Claas, J., Eskes, H. J., de Haan, J. F., Kleipool, Q., van Weele, M., Hasekamp, O., Hoogeveen, R., Landgraf, J., Snel, R., Tol, P., Ingmann, P., Voors, R., Kruizinga, B., Vink, R., Visser, H., and Levelt, P. F.: TROPOMI on the ESA Sentinel-5 Precursor: A GMES mission for global observations of the atmospheric composition for climate, air quality and ozone layer applications, *Remote Sensing of Environment*, 120, 70–83, <https://doi.org/10.1016/j.rse.2011.09.027>, 2012.
- 805 Verhoelst, T., Compernelle, S., Pinardi, G., Lambert, J. C., Eskes, H. J., Eichmann, K. U., Fjæraa, A. M., Granville, J., Niemeijer, S., Cede, A., Tiefengraber, M., Hendrick, F., Pazmiño, A., Bais, A., Bazureau, A., Folkert Boersma, K., Bogner, K., Dehn, A., Donner, S., Elokhov, A., Gebetsberger, M., Goutail, F., Grutter De La Mora, M., Gruzdev, A., Gratsea, M., Hansen, G. H., Irie, H., Jepsen, N., Kanaya, Y., Karagiozidis, D., Kivi, R., Kreher, K., Levelt, P. F., Liu, C., Müller, M., Navarro Comas, M., Piters, A. J., Pommereau, J. P., Portafaix, T., Prados-Roman, C., Puentedura, O., Querel, R., Remmers, J., Richter, A., Rimmer, J., Cárdenas, C. R., De Miguel, L. S., Sinyakov, V. P., Stremme, W., Strong, K., Van Roozendaal, M., Pepijn Veefkind, J., Wagner, T., Wittrock, F., Yela González, M., and Zehner, C.: Ground-based validation of the Copernicus Sentinel-5P TROPOMI NO₂ measurements with the NDACC ZSL-DOAS, MAX-DOAS and Pandora global networks, *Atmos. Meas. Tech.*, 14, 481–510, <https://doi.org/10.5194/amt-14-481-2021>, 2021.
- Vigouroux, C., Langerock, B., Augusto Bauer Aquino, C., Blumenstock, T., Cheng, Z., De Mazière, M., De Smedt, I., Grutter, M., Hannigan, J. W., Jones, N., Kivi, R., Loyola, D., Lutsch, E., Mahieu, E., Makarova, M., Metzger, J. M., Morino, I., Murata, I., Nagahama, T., Notholt, J., Ortega, I., Palm, M., Pinardi, G., Röhling, A., Smale, D., Stremme, W., Strong, K., Sussmann, R., Té, Y., Van Roozendaal, M., Wang, P., and Winkler, H.: TROPOMI-Sentinel-5 Precursor formaldehyde validation using an extensive network of ground-based Fourier-transform infrared stations, *Atmos. Meas. Tech.*, 13, 3751–3767, <https://doi.org/10.5194/amt-13-3751-2020>, 2020.
- 815 Vohra, K., Marais, E., Bloss, W. J., Schwartz, J., Mickley, L. J., Van Damme, M., Lieven, C., and Coheur, P.-F.: Rapid rise in premature mortality due to anthropogenic air pollution in fast-growing tropical cities from 2005 to 2018, *Science Advances*, 8, eabm4435, <https://doi.org/10.1126/sciadv.abm4435>, 2022.
- 820 Wagner, T., Deutschmann, T., and Platt, U.: Determination of aerosol properties from MAX-DOAS observations of the Ring effect, *Atmos. Meas. Tech.*, 2, 495–512, <https://doi.org/10.5194/amt-2-495-2009>, 2009.
- Williams, J. E., Folkert Boersma, K., Le Sager, P., and Verstraeten, W. W.: The high-resolution version of TM5-MP for optimized satellite retrievals: Description and validation, *Geoscientific Model Development*, 10, 721–750, <https://doi.org/10.5194/gmd-10-721-2017>, 2017.
- 825 Yombo Phaka, R., Merlaud, A., Pinardi, G., Mahieu, E., Hendrick, F., Friedrich, M. M., Fayt, C., Van Roozendaal, M., Djibi, B. L., Bopili Mbotia Lepiba, R., Phuku Phuati, E., and Mbungu Tsumbu, J.-P.: First Ground-Based Doas Measurements of No₂ At Kinshasa and Comparisons With Satellite Observations, *Journal of Atmospheric and Oceanic Technology*, pp. 1291–1304, <https://doi.org/10.1175/jtech-d-20-0195.1>, 2021.

- Zhao, X., Griffin, D., Fioletov, V., McLinden, C., Cede, A., Tiefengraber, M., Müller, M., Bogner, K., Strong, K., Boersma, F., Eskes, H.,
830 Davies, J., Ogyu, A., and Lee, S. C.: Assessment of the quality of tropomi high-spatial-resolution no2 data products in the greater toronto
area, *Atmos. Meas. Tech.*, 13, 2131–2159, <https://doi.org/10.5194/amt-13-2131-2020>, 2020.
- Zhu, L., Jacob, D. J., Mickley, L. J., Marais, E. A., Cohan, D. S., Yoshida, Y., Duncan, B. N., Abad, G. G., and Chance, K. V.: Anthropogenic
emissions of highly reactive volatile organic compounds in eastern Texas inferred from oversampling of satellite (OMI) measurements of
HCHO columns, *Environmental Research Letters*, 9, 114004, <https://doi.org/10.1088/1748-9326/9/11/114004>, 2014.

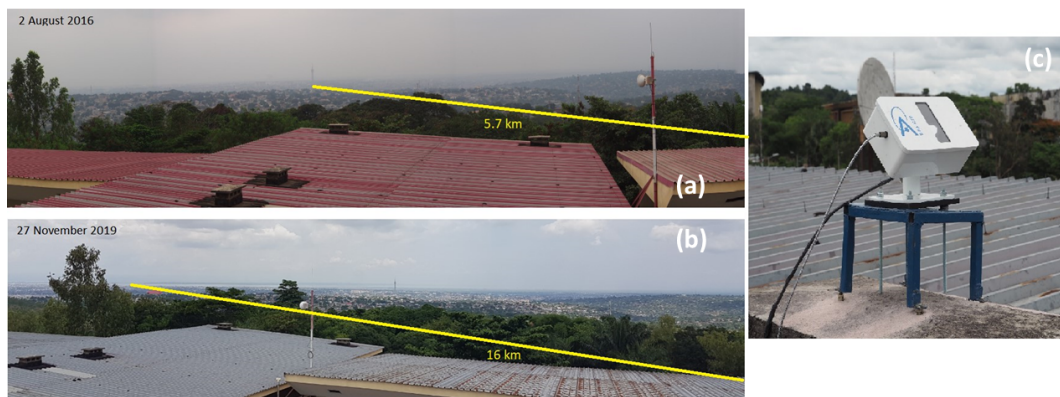
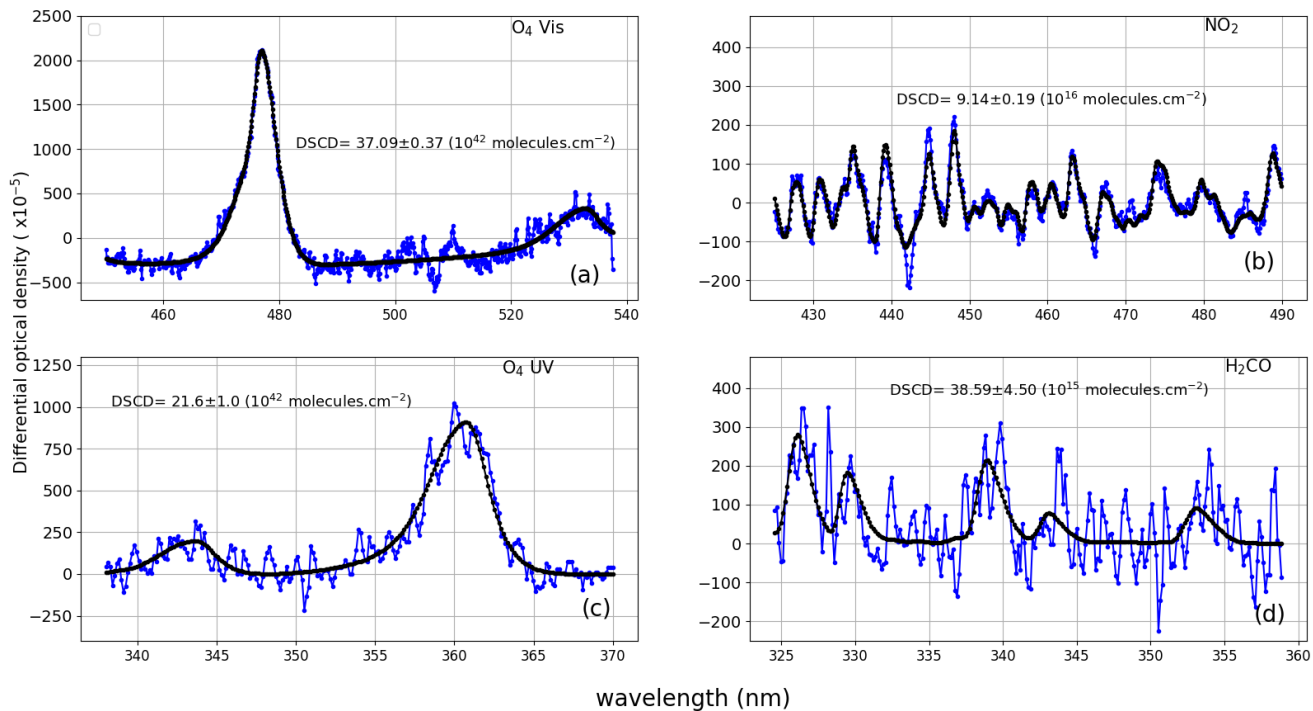


Figure 1. The MAX-DOAS instrument as installed on the roof of the Faculty of Science of the University of Kinshasa (panel c). The yellow lines (panels a and b) point respectively to the Lumumba tower, visible at 5.7 km from the site and the city of Brazzaville, visible at about 16 km on clear sky days.^{Add}



835

Figure 2 (Old): Example of QDOAS slant column retrievals for O_4 in the visible (panel a), NO_2 (panel b), O_4 in the ultraviolet (panel c) and H_2CO (panel d) for 20 February 2020 at 09h10 ...^{Del}

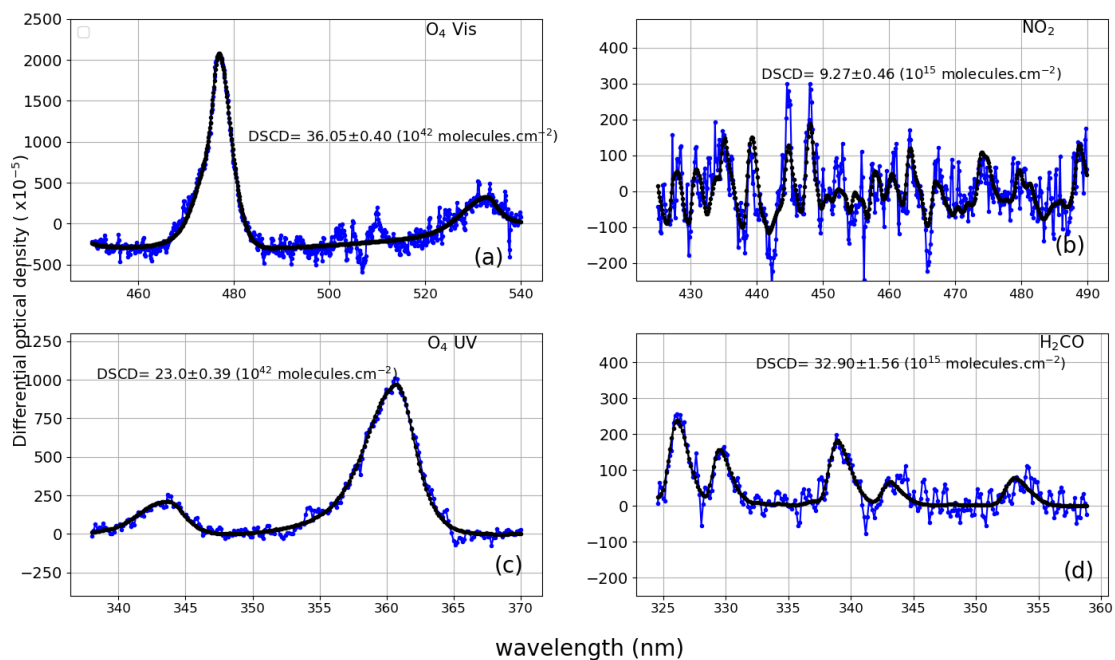


Figure 2. Example of QDOAS slant column retrievals for O_4 in the visible (panel a), NO_2 (panel b), O_4 in the ultraviolet (panel c) and H_2CO (panel d) for 20 February 2020 at 09h10 (Elevation viewing angle = 5°). Black lines correspond to molecular cross sections scaled to the detected absorptions and blue dots represent the measured signal.

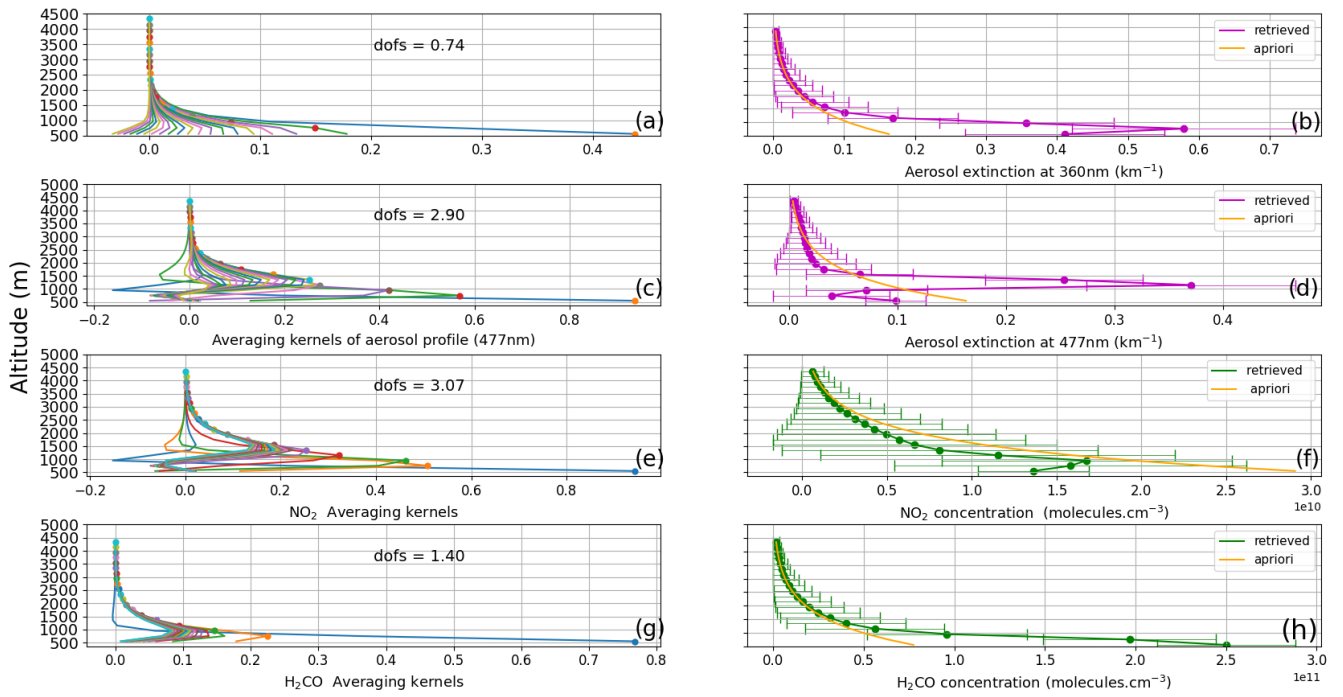


Figure 3 (Old): Example of FRM4DOAS products around 13h13 UTC ...^{Del}

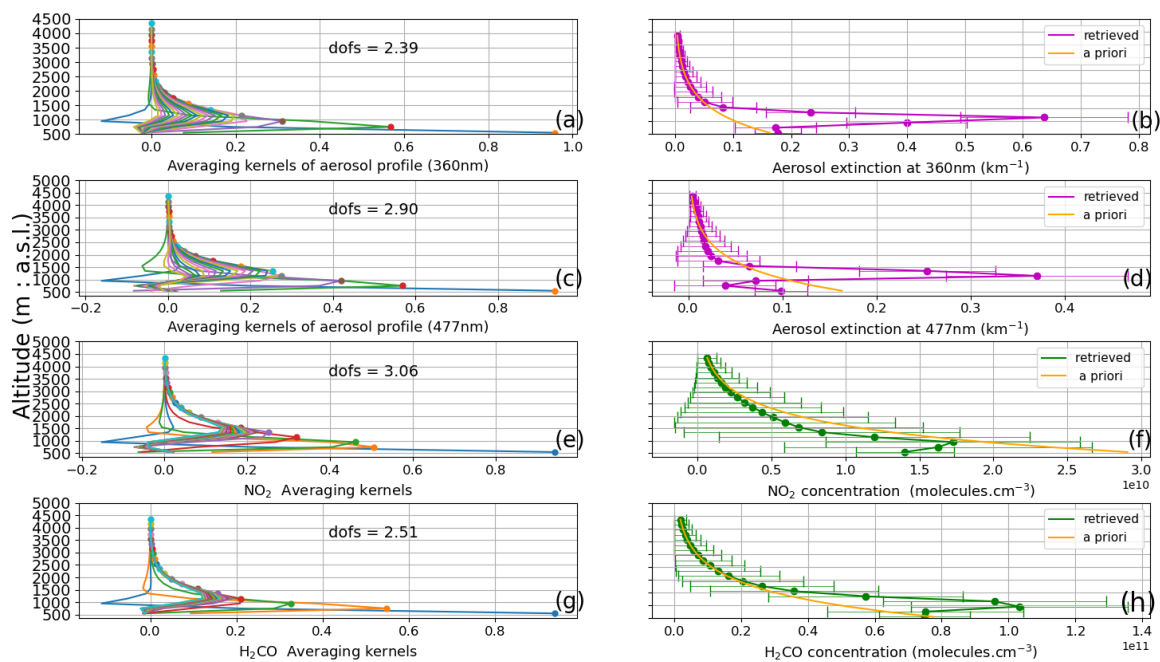


Figure 3. Example of FRM4DOAS products around 13h13 UTC of 13^{Del} 1^{Add} March 2020. The NO₂ and H₂CO profiles are represented in panels (f) and (h), respectively. Panels (e) and (g) show the corresponding Averaging Kernels (AKs), which are produced as part of the optical estimation inversion process and provide a measure of the vertical sensitivity of the measurements. Likewise, extinction profiles at 360 nm and 477 nm are represented in panels (b) and (d) and corresponding AKs are given in panels (a) and (c). The orange curves in the right subpanels are the a priori profiles. The horizontal bars represent the uncertainty on the retrieved profiles and, next to AKs, we also display values of the dofs (degree of freedom for signal).

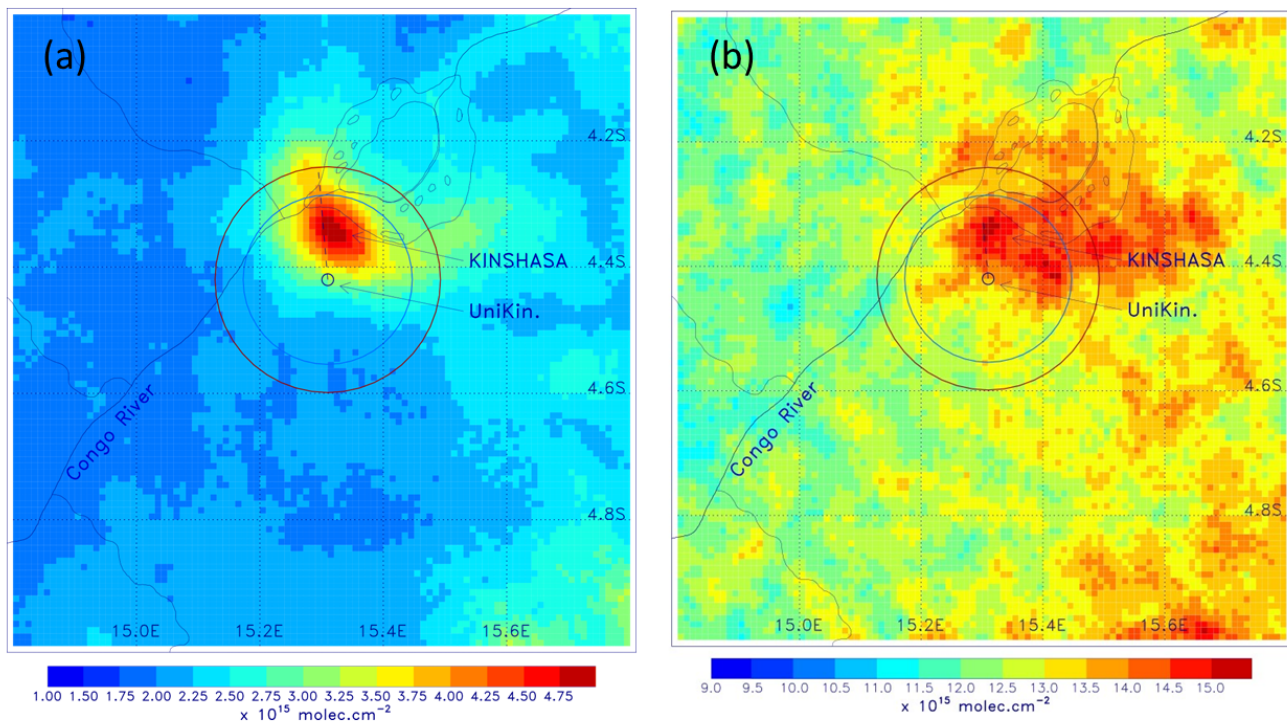


Figure 4. Distribution of oversampled NO₂ (panel a) and H₂CO (panel b) tropospheric columns in the station area (4°-5° S, 14.8°-15.8° E), from January 2020 to June 2021. The blue and brown circles represent the 15 km and 20 km radius circles around the station, respectively. The vertical black dashed line represents the pointing direction of the MAX-DOAS instrument.

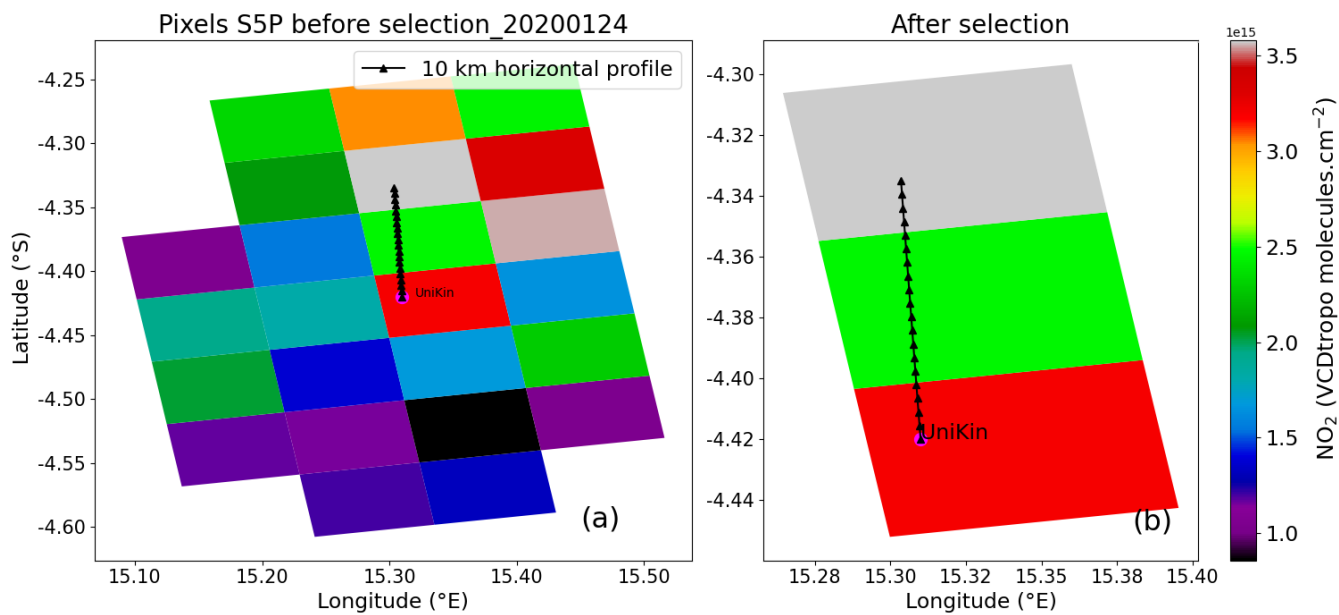


Figure 5. illustration of the approach taking into account the pixels along the MAX-DOAS viewing direction. Panel (a) shows all the pixels selected within a 20 km radius of the UniKin and panel (b) shows the pixels selected along the viewing direction shown as a black line. ^{Add}

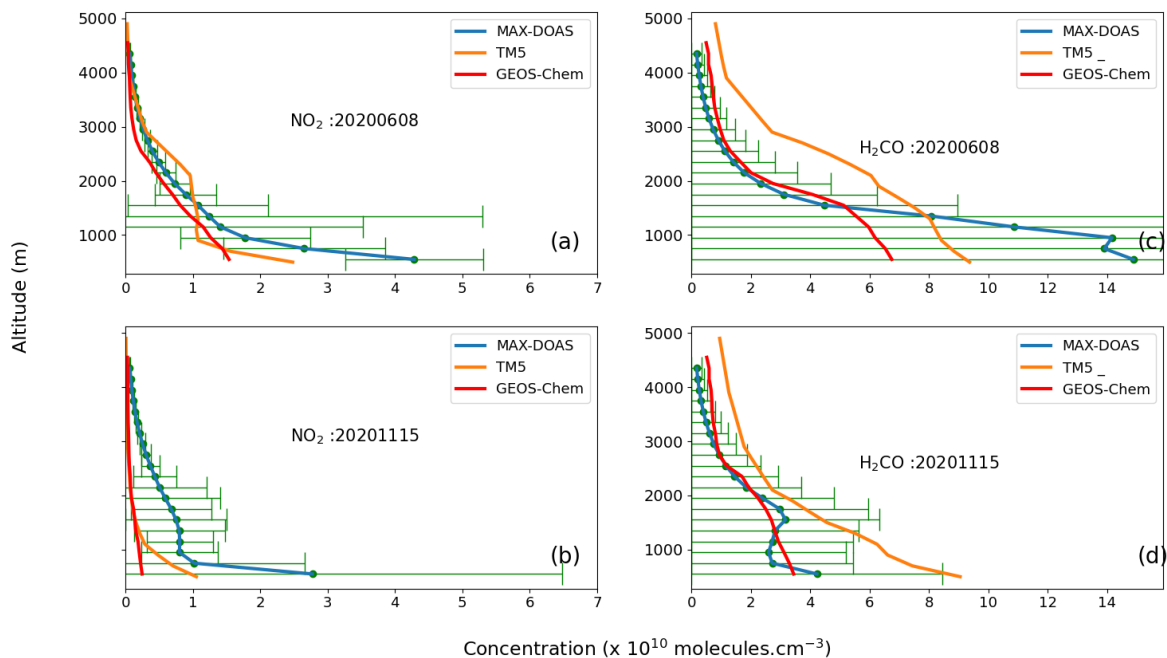


Figure 6. MAX-DOAS, TM5 and GEOS-Chem median profiles of NO₂ (panels: a, b) and H₂CO (panels : c, d). The error bars represent the standard deviation. The daily MAX-DOAS medians profiles shown in green dots are illustrated by the type of profile used to recalculate the tropospheric vertical column densities according to Eq.(1) and Eq. (2).^{Add}

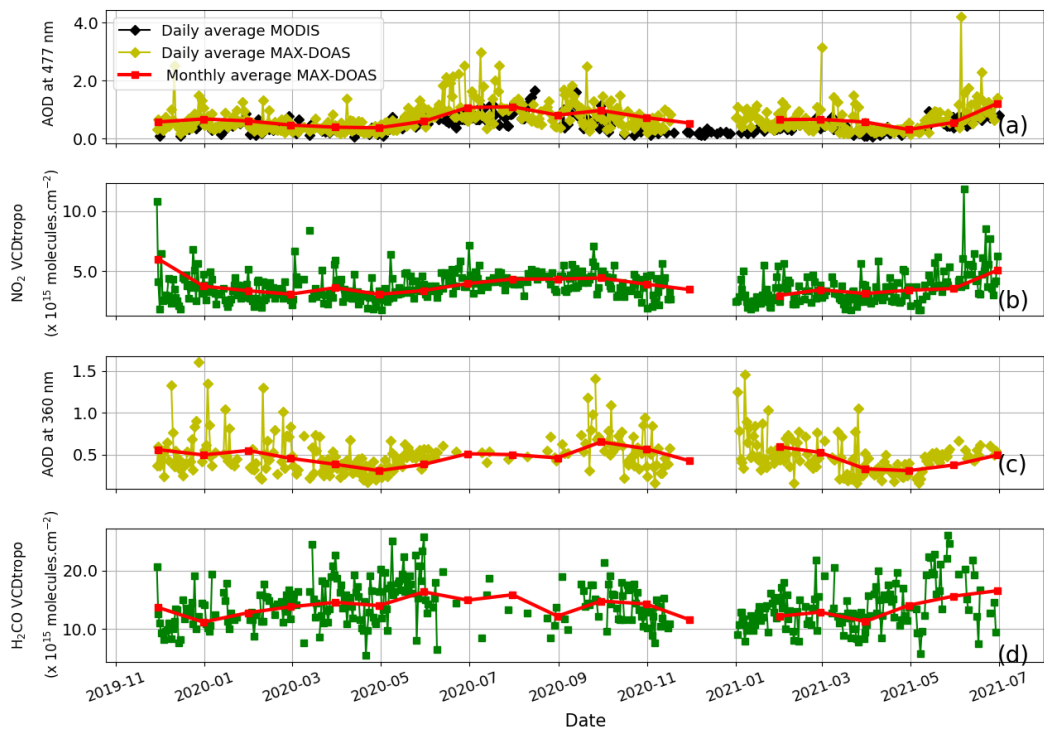


Figure 4 (Old): MAX-DOAS Aerosol optical depth (AOD) measured at 477 nm (panel a) and 360 nm (panel c) and VCD_{tropo} of NO_2 (panel b) and H_2CO (panel d) ...^{Del}

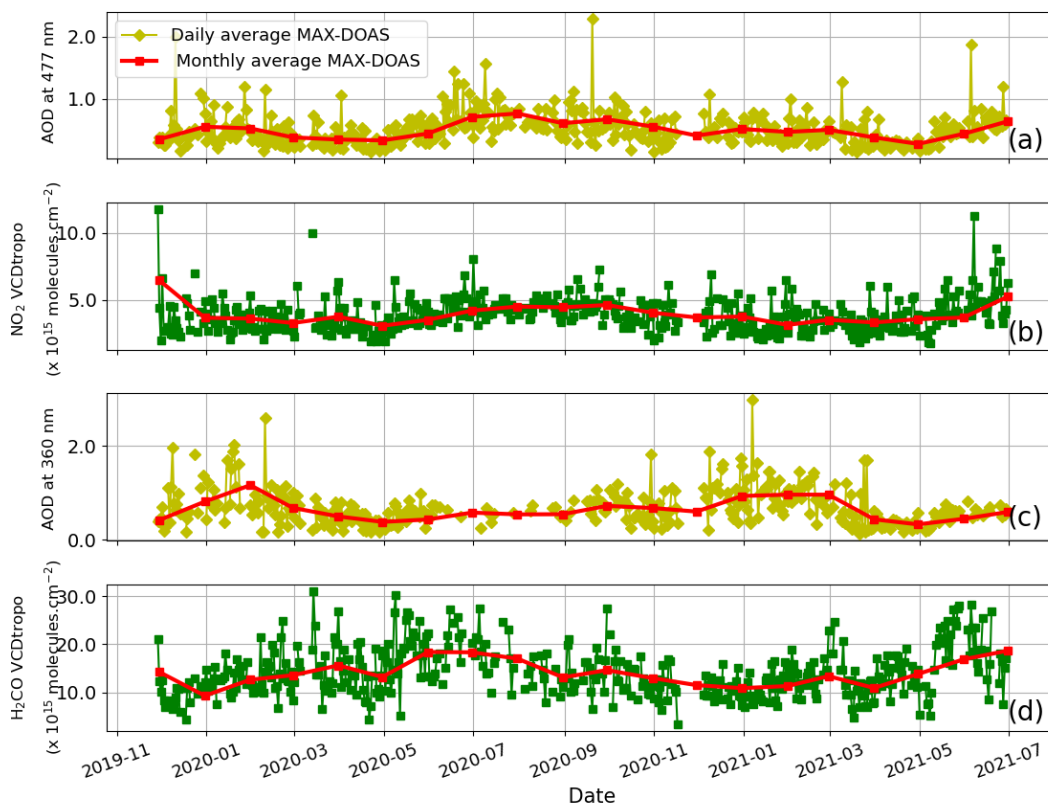
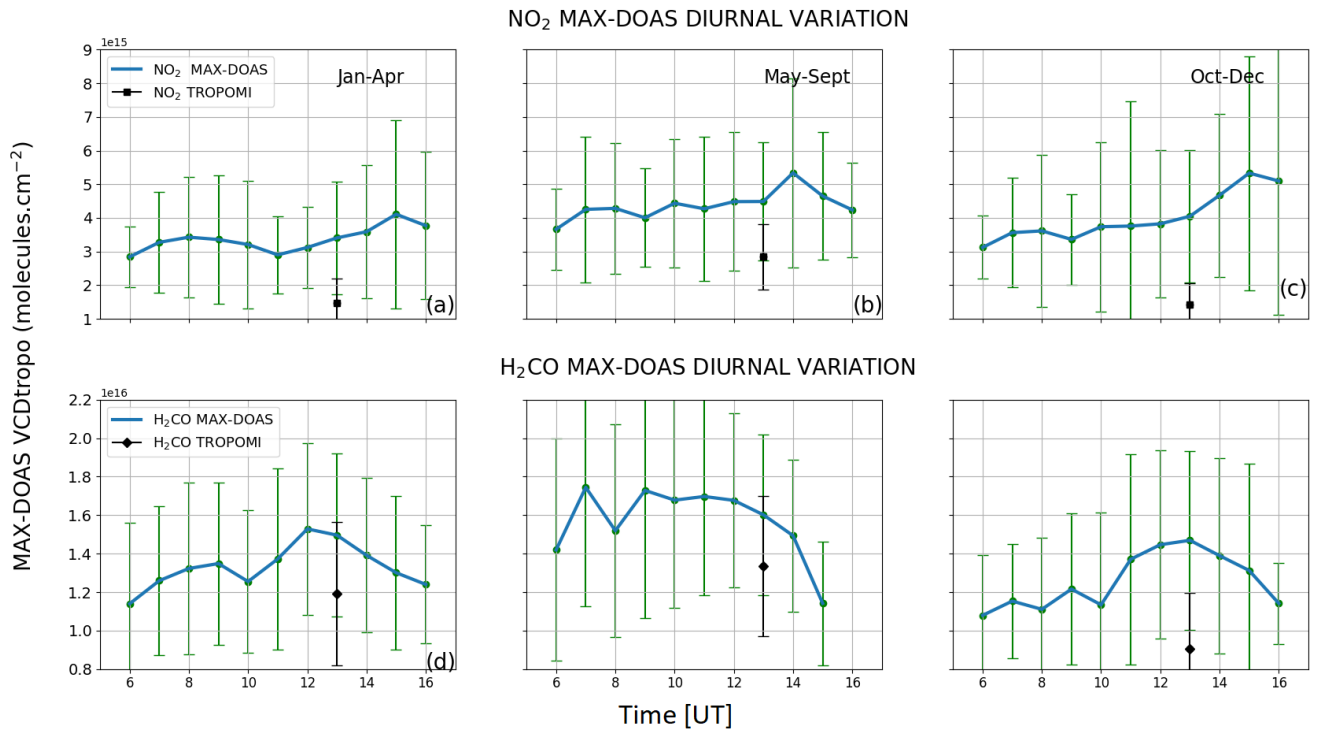


Figure 7. MAX-DOAS aerosol optical depth (AOD) measured at 477 nm (panel a) and 360 nm (panel c) and VCD_{tropo} of NO_2 (panel b) and H_2CO (panel d) measured between November 2019 and July 2021. Also in panel a is displayed the AOD observed at 550 nm wavelength by the MODIS Terra instrument (data downloaded from <https://giovanni.gsfc.nasa.gov/giovanni/> for an area covering the city of Kinshasa ($3-5^{\circ}S, 14-16^{\circ}E$).^{Del} In each panel, both daily and monthly averages are displayed.



840

Figure 5 (Old): Mean diurnal variations of NO₂ VCD_{tropo} (panels a, b, c) and H₂CO ...^{Del}

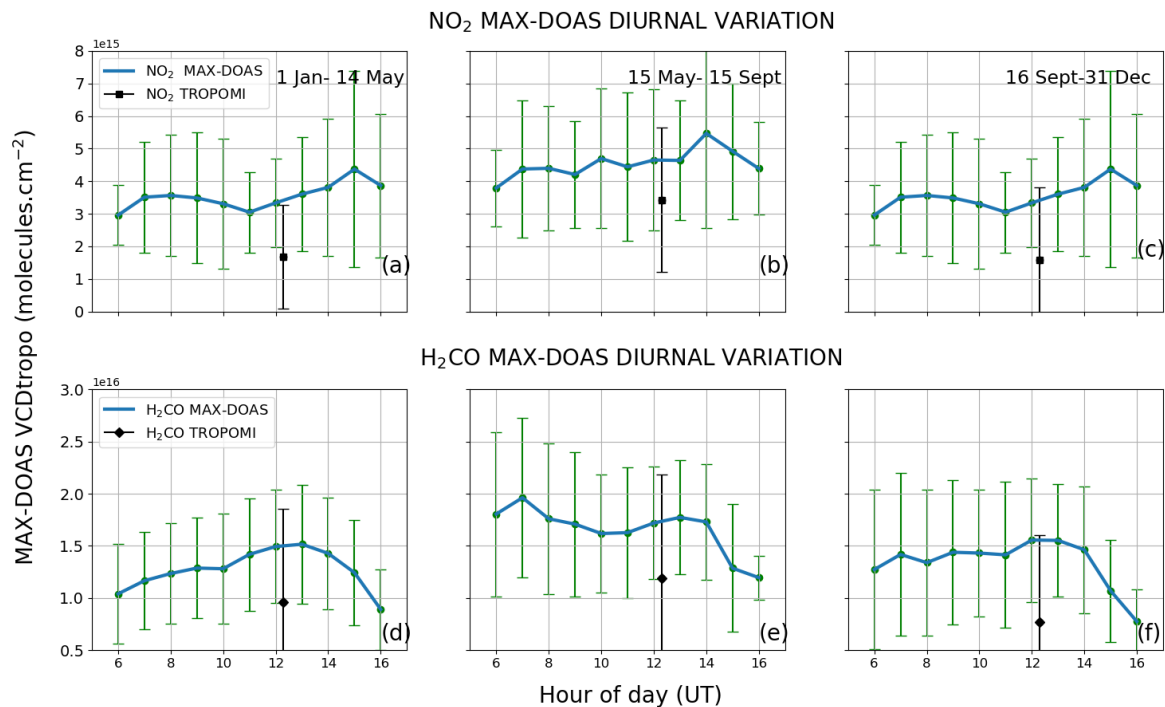


Figure 8. Mean diurnal variations of NO₂ VCD_{tropo} (panels a, b, c) and H₂CO (panels d, e, f) observed by the MAX-DOAS instrument (blue dots) and by TROPOMI (black dots) over the city of Kinshasa between November 2019 and July 2021. The error bars represent the (1- σ) standard deviation of VCD_{tropo} computed for each hour within the specified period.^{Add}

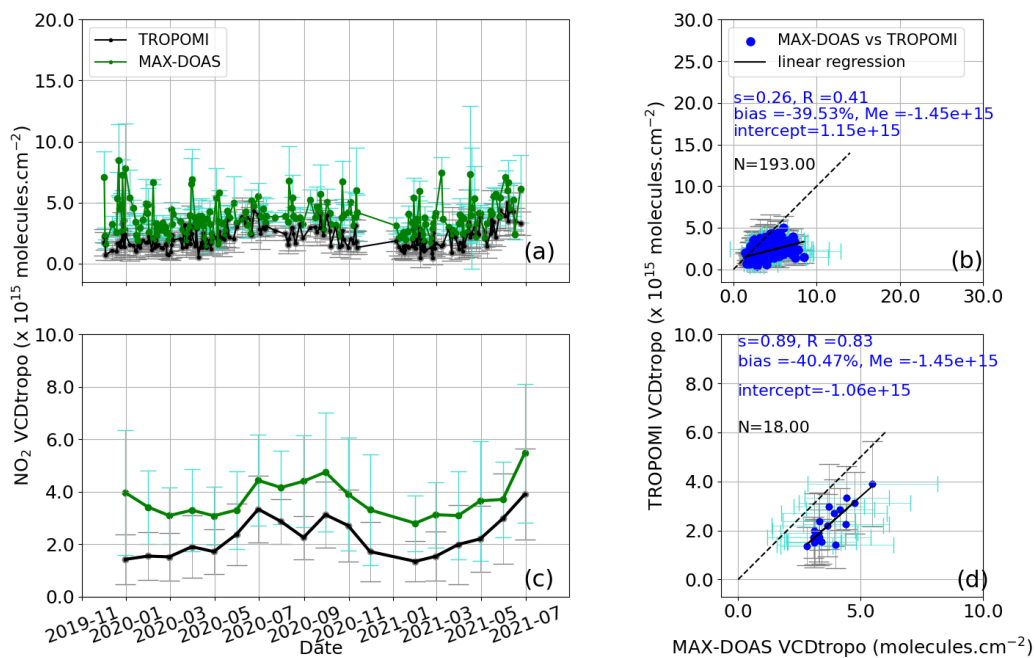


Figure A1 (Old): NO₂ Comparison of daily (panel a) and monthly (panel c) of tropospheric vertical column densities of MAX-DOAS (green dots) and TROPOMI (black dots) over Kinshasa from 1 November 2019 to 1 July 2021....^{Del}

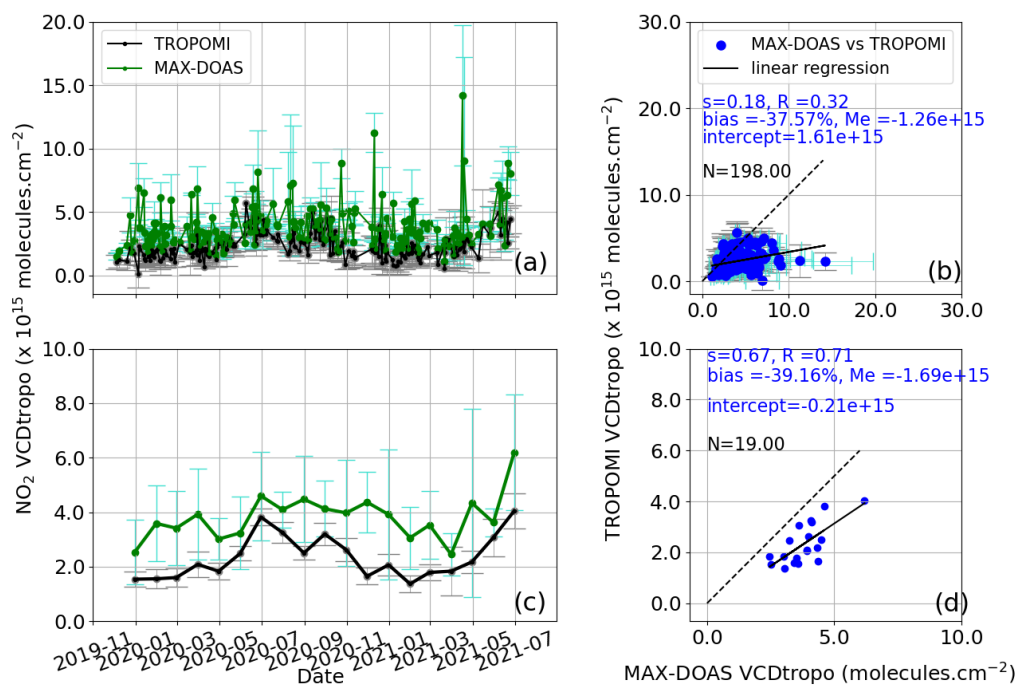


Figure 9. CASE 1 : NO₂ comparison of daily (panel a) and monthly (panel c) tropospheric vertical column densities of MAX-DOAS (green dots) and TROPOMI (black dots) over Kinshasa from 1 November 2019 to 1 July 2021. "Me" denotes the median bias^{Add}. ~~The MAX-DOAS are temporally averaged around the TROPOMI satellite overpass.~~^{Del} The MAX-DOAS is the hourly average coincidence day of TROPOMI satellite overpass.^{Add} Error bars are (1-σ) standard deviations. (panel b and d): least-squares^{Add} linear regressions between the two datasets.

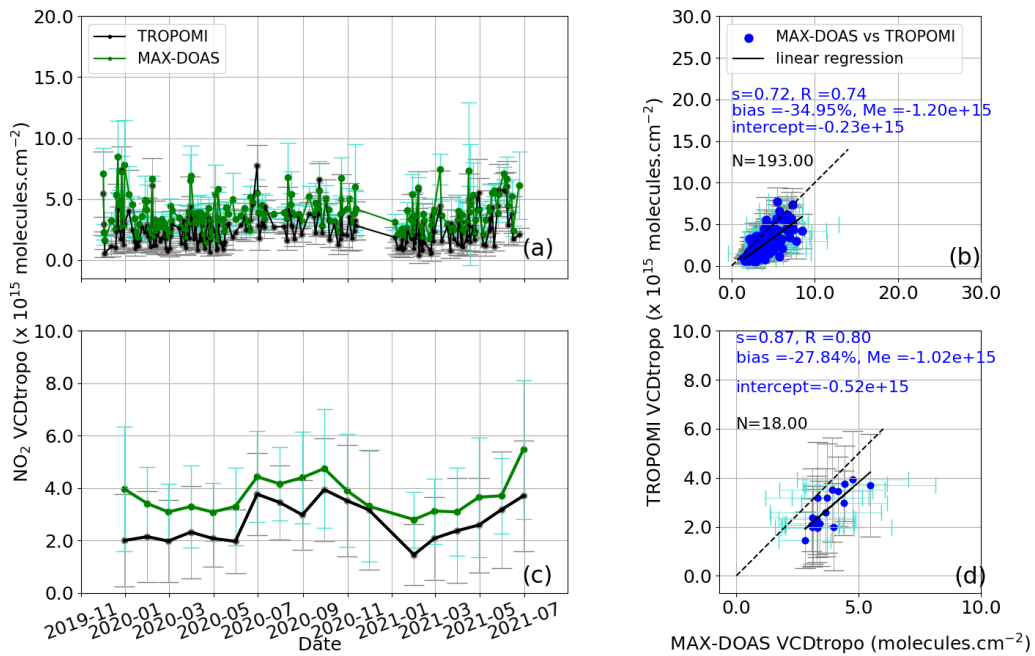


Figure A2 (Old): NO₂ Comparison of daily (panel a) and monthly (panel c) of tropospheric vertical column densities of MAX-DOAS (green dots) and TROPOMI (black dots) over Kinshasa from 1 November 2019 to 1 July 2021....^{Del}

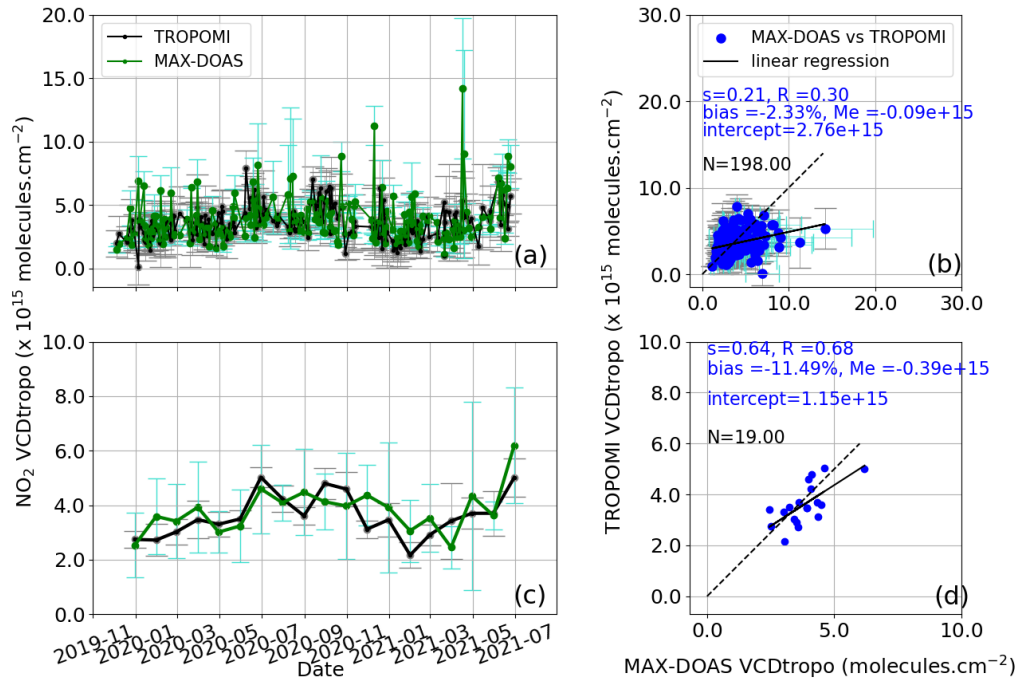
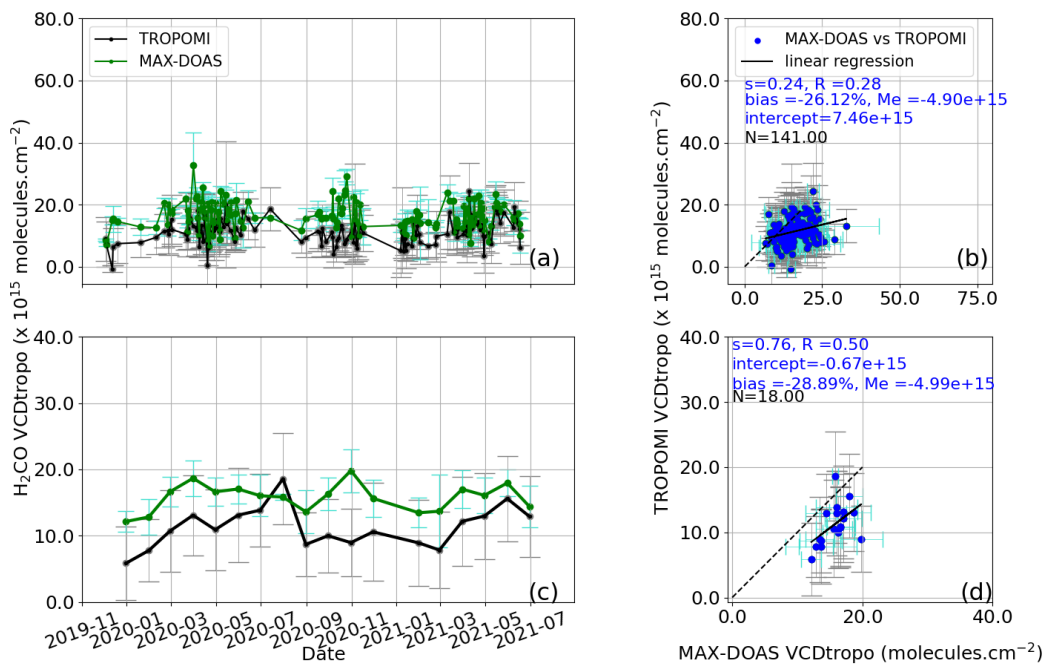


Figure 10. CASE 2 : NO₂ comparison of daily (panel a) and monthly (panel c) tropospheric vertical column densities of MAX-DOAS (green dots) and TROPOMI (black dots) over Kinshasa from 1 November 2019 to 1 July 2021. "Me" denotes the median bias median bias^{Add}. ~~The MAX-DOAS are temporally averaged around the TROPOMI satellite overpass.~~^{Del} The MAX-DOAS is the hourly average coincidence day of TROPOMI satellite overpass.^{Add} The individual TROPOMI points are those obtained from formulas 1 and 2 as described in the second case. Error bars are the standard deviations. (panel b and d): least-squares^{Add} linear regressions between the two datasets.



845

Figure B1 (Old): CASE 1: H_2CO Comparison of daily (panel a) and monthly (panel c) of tropospheric vertical column densities of MAX-DOAS (green dots) and TROPOMI (black dots) over Kinshasa from 1 November 2019 to 1 July 2021....^{Del}

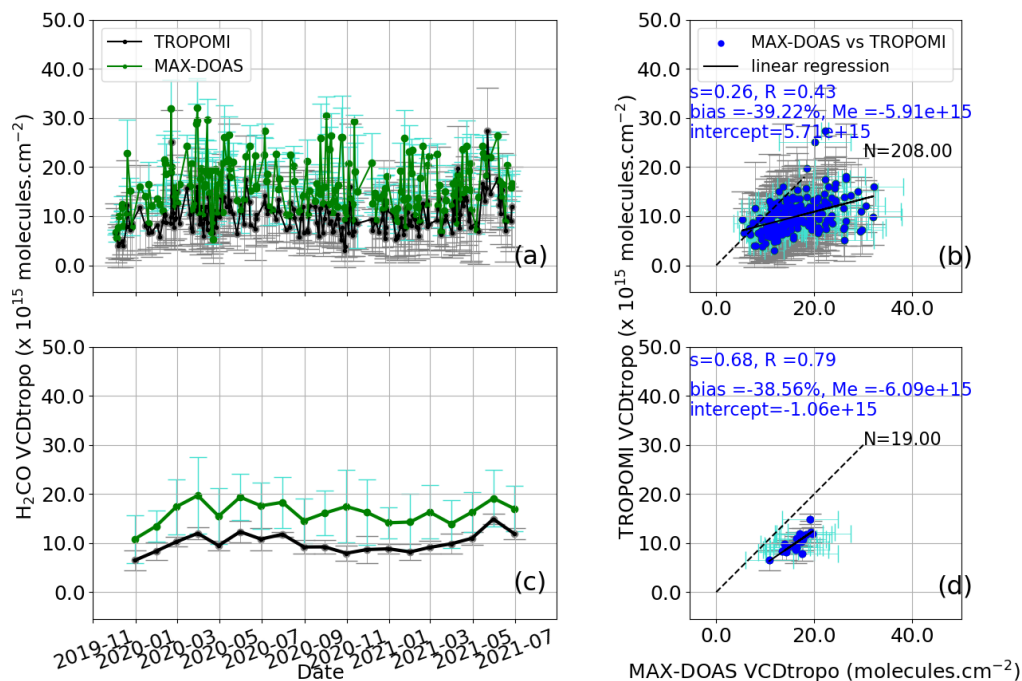


Figure 11. CASE 1 : H₂CO comparison of daily (panel a) and monthly (panel c) tropospheric vertical column densities of MAX-DOAS (green dots) and TROPOMI (black dots) over Kinshasa from 1 November 2019 to 1 July 2021. "Me" denotes the median bias^{Add}. ~~The MAX-DOAS are temporally averaged around the TROPOMI satellite overpass.~~^{Del} The MAX-DOAS is the hourly average coincidence day of TROPOMI satellite overpass.^{Add} Error bars are (1- σ) standard deviations. (panel b and d): least-squares^{Add} linear regressions between the two datasets.

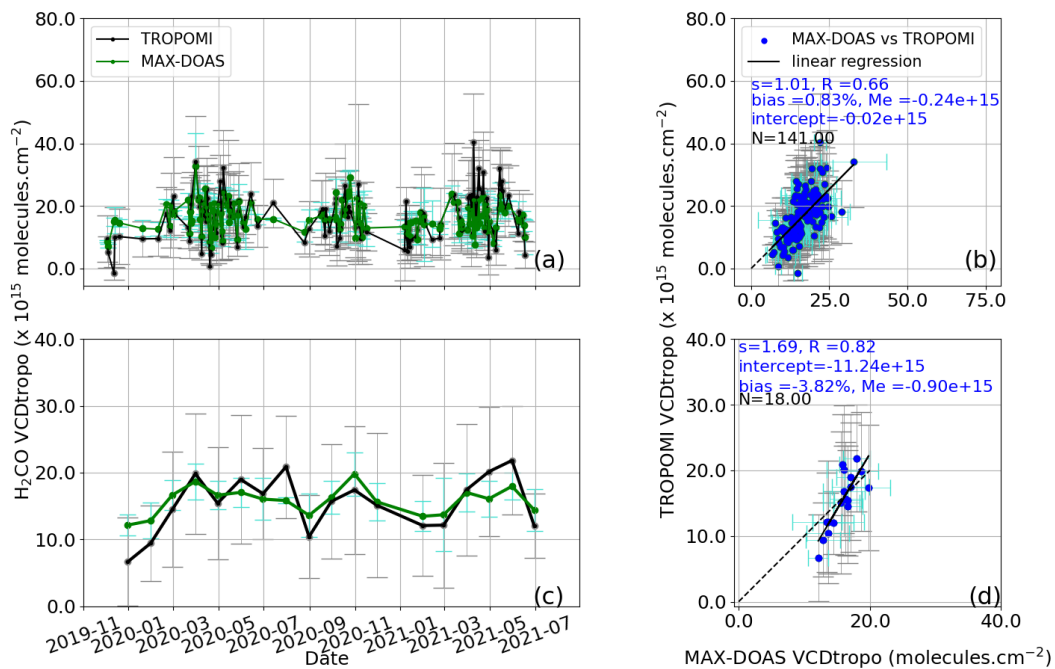


Figure B2 (Old): H₂CO Comparison of daily (panel a) and monthly (panel c) of tropospheric vertical column densities of MAX-DOAS (green dots) and TROPOMI (black dots) over Kinshasa from 1 November 2019 to 1 July 2021....^{Del}

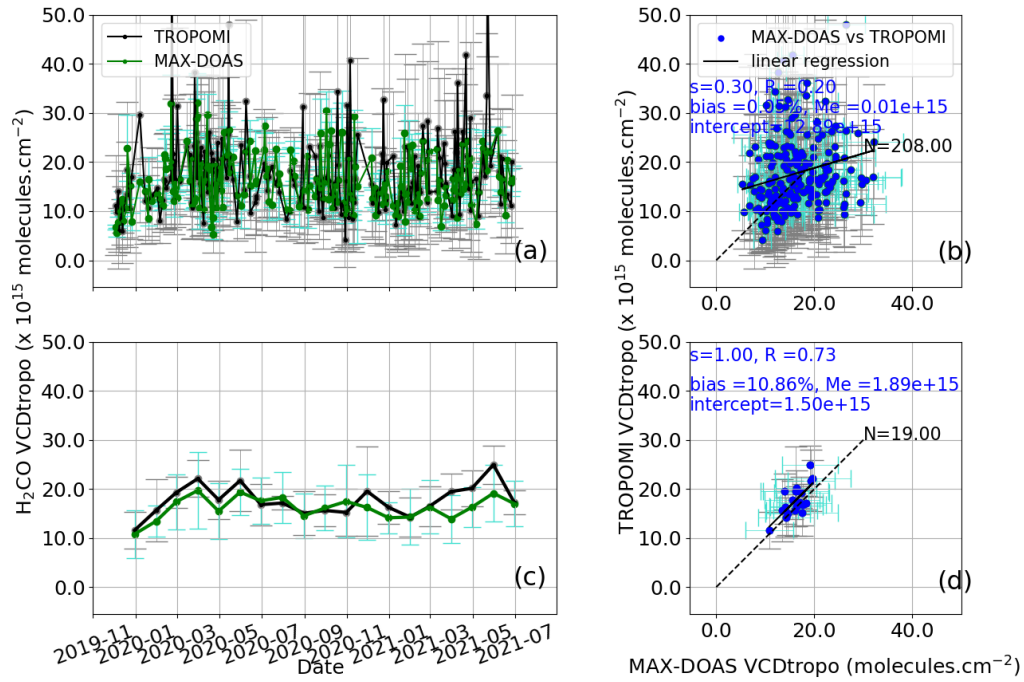


Figure 12. CASE 2 : H₂CO comparison of daily (panel a) and monthly (panel c) tropospheric vertical column densities of MAX-DOAS (green dots) and TROPOMI (black dots) over Kinshasa from 1 November 2019 to 1 July 2021. "Me" denotes the median bias median bias^{Add}. ~~The MAX-DOAS are temporally averaged around the TROPOMI satellite overpass.~~^{Del} The MAX-DOAS is the hourly average coincidence day of TROPOMI satellite overpass.^{Add} The individual TROPOMI points are those obtained from formulas 1 and 2 as described in the second case. Error bars are the standard deviations. (panel b and d): least-squares^{Add} linear regressions between the two datasets.

Table 1. Main QDOAS analytical parameters for the retrieval of NO₂ and H₂CO DSCD

Parameters	NO ₂ Settings	H ₂ CO Settings
Fitting interval	425-490nm	325-360nm
Calibration	Chance and Kurucz (2010)	
NO ₂	Vandaele et al. (1998), 298K	
O ₃	Bogumil et al. (2003), 223K	Serdyuchenko et al. (2014), 223K and 243K
H ₂ O	Harder and Brault (1997)	-
O ₄	Hermans et al. (2003)	Thalman and Volkamer (2013), 293K
H ₂ CO	-	Meller and Moortgat (2000), 293K
BrO	-	Fleischmann et al. (2004), 223K
Correction ring effet	Chance and Spurr (1997)	
polynomial Term	Polynomial of order 5	
Offset intensity correction	Offset(constant), offset(order1) « Non-linear »	

Table 2. MMF retrieval settings for NO₂ and H₂CO observation in Kinshasa

Parameters	NO ₂ Settings	H ₂ CO Settings
Surface albedo	0.06	0.06
Angström exponent	1	1
Wavelengths	477 nm	360 nm
Pressure and temperature profile	climatology from ECMWF 1995–2016	
A priori profile	exponential decay with a scale height of 1km	
Covariance a priori ^{Add}	diagonal elements as x_a^2 , correlation length of 0.2 km ^{Add}	
VCD _{tropo} apriori	3×10^{15} molecules cm ⁻²	8×10^{15} molecules cm ⁻²
Single aerosol scattering albedo	0.92	0.92
Aerosol optical depth apriori	0.18	0.18
Asymmetry parameter	0.68	0.68
Height grid	200 m spacing up to 4 km	

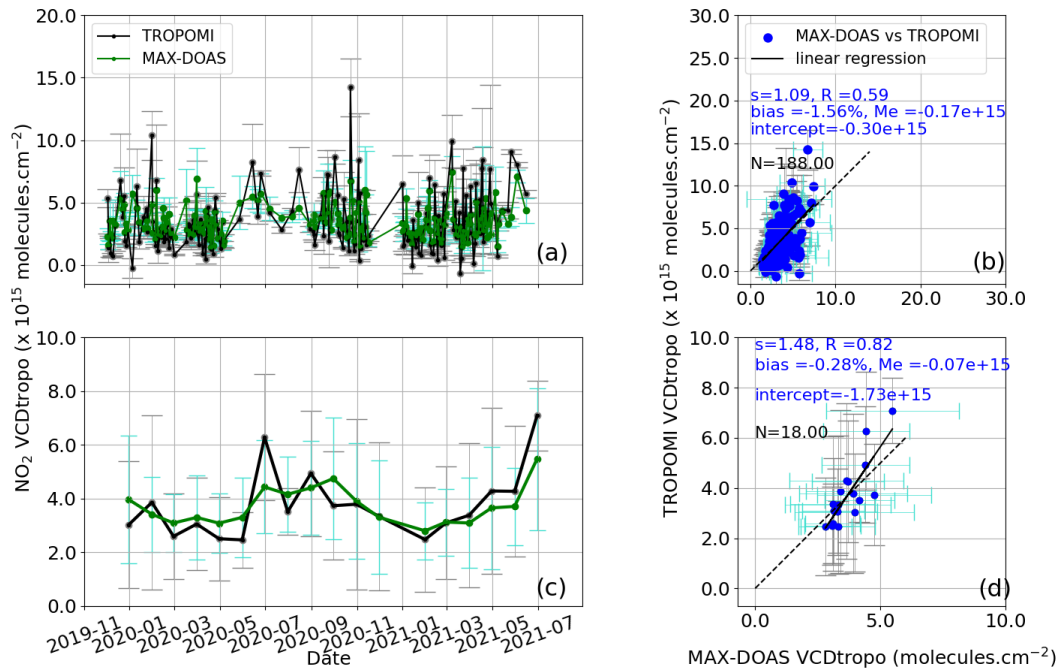
Table 3. Statistics summary for the MAX-DOAS and TROPOMI NO₂ comparisons.

Approach	s ; R ; intercept and bias (daily average)	s ; R ; intercept and bias (monthly average)
Case 1 : Direct comparison, all pixels^{Del}	0.26 ; 0.41 ; -1.15×10^{15} ; -40 %^{Del}	0.89 ; 0.83 ; -1.61×10^{15} ; -40 %^{Del}
Case 1 : Direct comparison, all pixels ^{Add}	0.18 ; 0.32 ; 1.61×10^{15} ; -38 % ^{Add}	0.67 ; 0.71 ; -0.21×10^{15} ; -39 % ^{Add}
Case 2 : Recalculated TROPOMI, all pixels^{Del}	0.72 ; 0.74 ; -0.23×10^{15} ; -35 %^{Del}	0.87 ; 0.80 ; -0.52×10^{15} ; -28 %^{Del}
Case 2 : Recalculated TROPOMI, all pixels ^{Add}	0.21 ; 0.30 ; 2.76×10^{15} ; -2 % ^{Add}	0.64 ; 0.68 ; 1.15×10^{15} ; -12 % ^{Add}
Case 3 : Recalculated TROPOMI, azimuth-based selection^{Del}	1.09 ; 0.59 ; -0.30×10^{15} ; -2 %^{Del}	1.48 ; 0.82 ; -1.73×10^{15} ; -0.28 %^{Del}
Case 3 : Recalculated TROPOMI, azimuth-based selection ^{Add}	0.42 ; 0.43 ; 3.87×10^{15} ; 41 % ^{Add}	0.77 ; 0.48 ; 2.74×10^{15} ; 44 % ^{Add}

Table 4. Statistics summary for the MAX-DOAS and TROPOMI H₂CO comparisons.

Approach	s ; R ; intercept and bias (daily average)	s ; R ; intercept and bias (monthly average)
Case 1 : Direct comparison, all pixels^{Del}	0.24 ; 0.28 ; 7.46×10^{15} ; -26 %^{Del}	0.76 ; 0.50 ; -0.67×10^{15} ; -29 %^{Del}
Case 1 : Direct comparison, all pixels ^{Add}	0.26 ; 0.43 ; 5.71×10^{15} ; -39 % ^{Add}	0.68 ; 0.79 ; -1.06×10^{15} ; -39 % ^{Add}
Case 2 : Recalculated TROPOMI, all pixels^{Del}	1.01 ; 0.66 ; -0.02×10^{15} ; 1 %^{Del}	1.69 ; 0.82 ; -11.24×10^{15} ; -4 %^{Del}
Case 2 : Recalculated TROPOMI, all pixels ^{Add}	0.30 ; 0.20 ; 12.89×10^{15} ; 0.05 % ^{Add}	1.00 ; 0.73 ; 1.50×10^{15} ; 11 % ^{Add}
Case 3 : Recalculated TROPOMI, azimuth-based selection^{Del}	1.51 ; 0.60 ; -5.79×10^{15} ; 13 %^{Del}	1.78 ; 0.52 ; -8.98×10^{15} ; 17 %^{Del}
Case 3 : Recalculated TROPOMI, azimuth-based selection ^{Add}	0.37 ; 0.25 ; 12.61×10^{15} ; 5 % ^{Add}	0.90 ; 0.55 ; 3.15×10^{15} ; 4 % ^{Add}

Appendix A: NO₂ Intercomparison of TROPOMI with MAX-DOAS : case case 3



850 **Figure 7 (Old): CASE 3 : NO₂ comparison of daily (panel a) and monthly (panel c) of tropospheric vertical column densities of MAX-DOAS (green dots) and TROPOMI (black dots) over Kinshasa from 1 November 2019 to 01 July 2021...**^{Del}

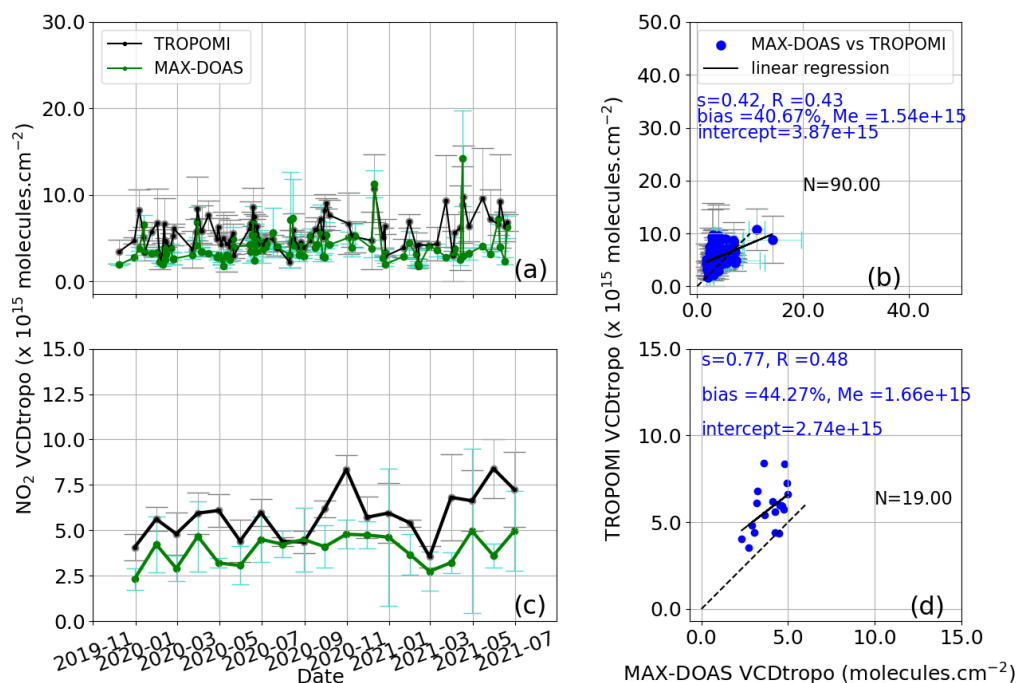


Figure A1. CASE 3 : NO_2 comparison of daily (panel a) and monthly (panel c) tropospheric vertical column densities of MAX-DOAS (green dots) and TROPOMI (black dots) over Kinshasa from 1 November 2019 to 01 July 2021. "Me" denotes the median bias median bias^{Add}. ~~The MAX-DOAS are temporally averaged around the TROPOMI satellite overpass.~~^{Del} The MAX-DOAS is the hourly average coincidence day of TROPOMI satellite overpass.^{Add} The individual TROPOMI points are those obtained from formulas 1 and 2. TROPOMI error bars are standard deviations. Panel b and panel d are results of least-squares^{Add} linear regressions between the two datasets, and provide the corresponding statistics.

Appendix B: H₂CO Intercomparison of TROPOMI with MAX-DOAS : case 3

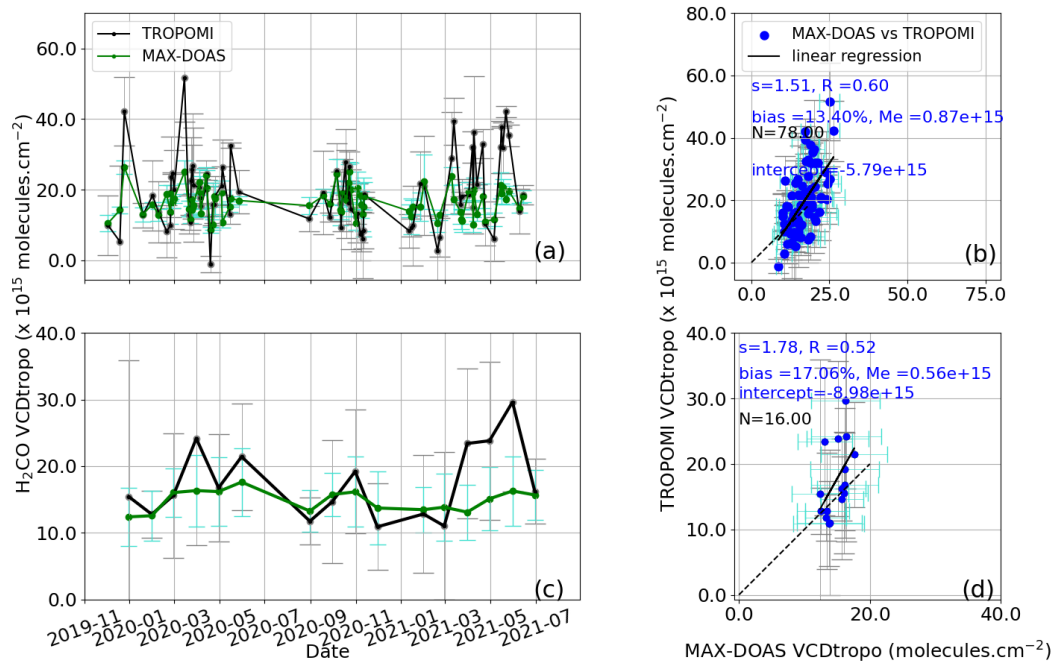


Figure 10 (Old): CASE 3 : H₂CO Comparison of daily (panel a) and monthly (panel c) of tropospheric vertical column densities of MAX-DOAS (green dots) and TROPOMI (black dots) over Kinshasa from November 1, 2019 to July 01, 2021.

855

...Del

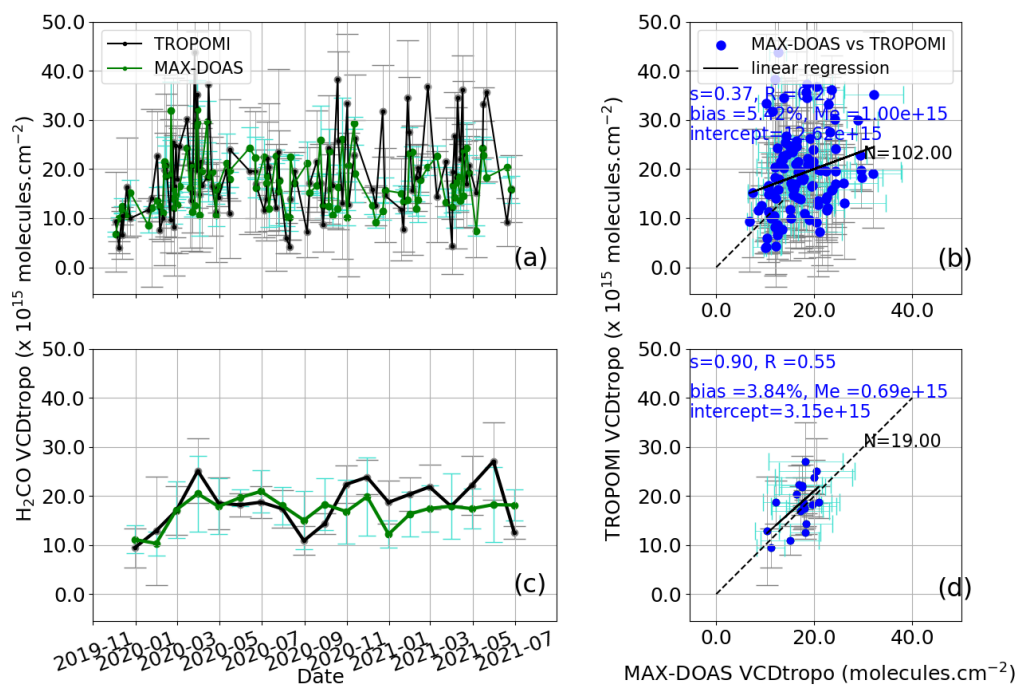


Figure B1. CASE 3 : H₂CO Comparison of daily (panel a) and monthly (panel c) tropospheric vertical column densities of MAX-DOAS (green dots) and TROPOMI (black dots) over Kinshasa from November 1, 2019 to July 01, 2021. "Me" denotes the median bias median bias^{Add}. ~~The MAX-DOAS are temporally averaged around the TROPOMI satellite overpass.~~^{Del} The MAX-DOAS is the hourly average coincidence day of TROPOMI satellite overpass.^{Add} The individual TROPOMI points are those obtained from formulas 1 and 2. TROPOMI error bars are standard deviations. Panel b and panel d show the results of least-squares^{Add} linear regressions between the two datasets.

Appendix C: median profiles

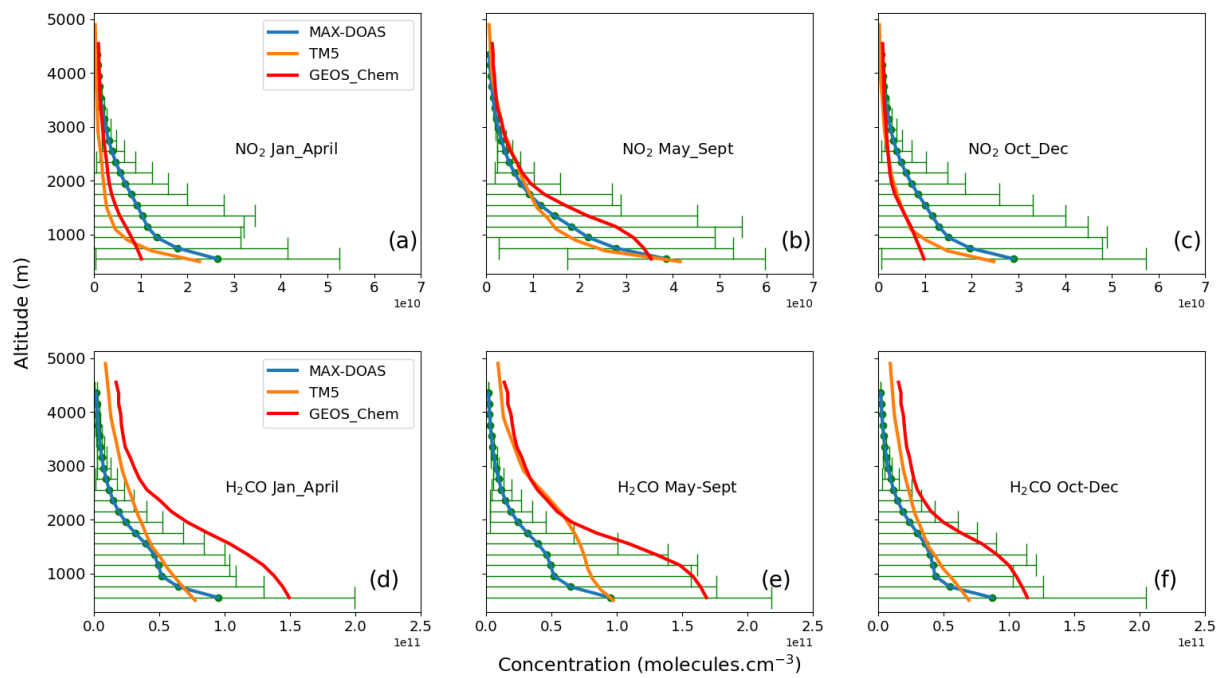


Figure C1. MAX-DOAS, TM5 and GEOS-Chem median profiles of NO₂ (panels: a, b, c) and H₂CO (panels : d, e, f). The error bars represent the standard deviation.

Appendix D: AOD MODIS

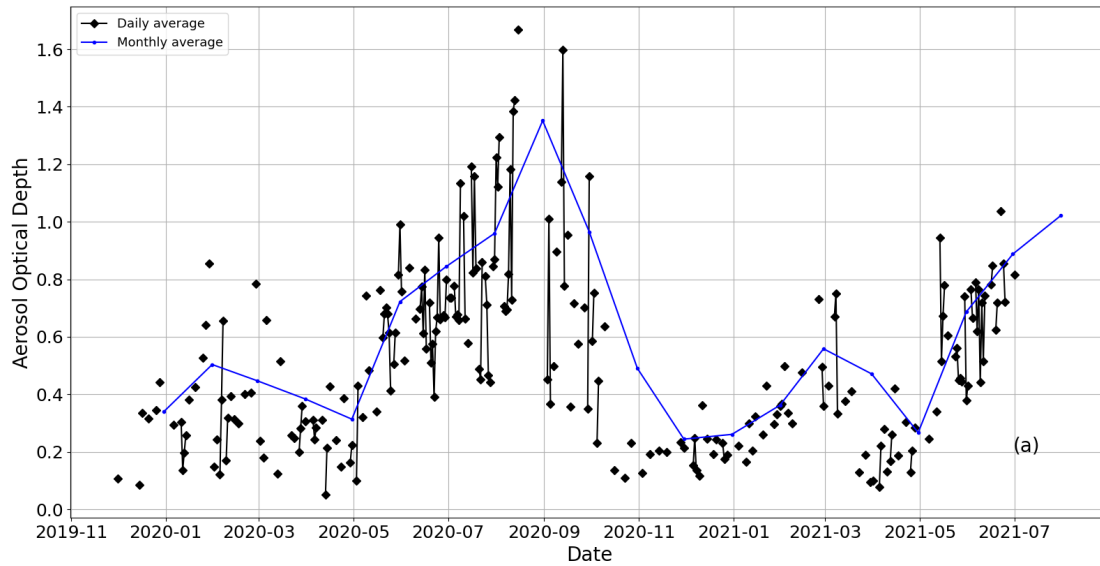


Figure D1. Time series of the monthly aerosol optical depth (AOD) observed at 550 nm wavelength by the MODIS Terra instrument downloaded from <https://giovanni.gsfc.nasa.gov/giovanni/> for an area covering the city of Kinshasa (3–5°S, 14–16°E).^{Add}